DISEASES AND DISORDERS

Rapid and high-sensitivity screening of pregnancy complications by profiling circulating placental extracellular vesicles

Carlos Palma[1,2]†, Mostafa Kamal Masud[2,3]†, Dominic Guanzon[1,2], Andrew Lai[1,2], Melissa Razo[1,2], Angela Nakahara[4], Soumyalekshmi Nair[1], Alexis Salas-Burgos[5], Md Shahriar A. Hossain[3,6], Flavio Carrion[7], Gregory Duncombe[1,2], H. David McIntyre[8], Aase Handberg[9], Sherri Longo[3], Yusuke Yamauchi[2,3,10]*, Carlos Salomon[1,2]*

Herein, we developed a specific, rapid sensor to quantify placental extracellular vesicle (EV) protein biomarkers of early pregnancy complications. A distinct tetraspanin CD9 and placental alkaline phosphatase (PLAP) expression pattern was observed via targeted multiple reaction monitoring of EVs from maternal plasma collected before 18 weeks of gestation. A classification model was developed using training and validation patient sets, distinguishing between individuals at high risk of developing complications from those with normal pregnancies, achieving 80% sensitivity, 90% specificity, 89% positive predictive value (PPV), and 82% negative predictive value (NPV). Superparamagnetic nanoflowers that captured target EVs ($CD9^+$/$PLAP^+$) were used to construct a 4-flex glass strip nanozymatic readout system. The sensor analyzes plasma for EVs, identifying gestational diabetes mellitus risk with a 95% combined sensitivity, 100% specificity, 100% PPV, and 96% NPV. This nanoplatform identifies individuals at risk of developing pregnancy complications with a >90% classification accuracy, exhibiting potential for clinical applications.

INTRODUCTION

Pregnancy complications that compromise fetal development have profound effects on pregnancy outcomes and the life-long disease risk susceptibility of the offspring (*1*, *2*). One of the most notable changes throughout pregnancy occurs in the endocrine system, a source of important hormones and protective tissue barrier, ensuring proper fetal development (*3*, *4*). Common pregnancy complications include gestational hypertension, gestational diabetes mellitus (GDM), maternal systemic inflammation, infections, premature delivery, and fetal growth restriction (*5*). Moreover, certain congenital anomalies that occur during fetal development, such as structural chromosomal abnormalities, heart defects, and neural tube defects, can negatively affect pregnancy progression (*6*, *7*). These complications can also lead to maternal health issues, such as hypertension and diabetes after childbirth (*8*, *9*). Now, the diagnosis of these conditions relies primarily on blood tests, ultrasound screening, blood pressure (BP) monitoring, proteinuria tests for hypertension and preeclampsia (PE) (*2*), and oral glucose challenge tolerance test (OGTT) for GDM (*1*). Although these methods are generally reliable, anomalies may not be detected early enough to ensure favorable outcomes with timely clinical interventions. Due to the increasing occurrence of perinatal morbidity and mortality linked to pregnancy complications, it is critical to develop screening tools capable of promptly and precisely diagnosing pregnancy-related complications and fetal abnormalities.

Extracellular vesicle (EV) signaling is a growing area of clinical research that offers opportunities (*10*) for generating data on cell communication systems, identifying tissue-specific biomarkers, and developing naïve and engineered endogenous EV- and synthetic EV–based therapeutics and drug delivery systems (*11*). These opportunities have arisen because of a paradigm shift in our understanding of how cells communicate, particularly the recognition of the role of EVs in intercellular signaling, with particular interest in endocrinology (*12*). EVs are stable lipid bilayer vesicles packaged with tissue-specific signaling molecules capable of regulating proximal and distal cell functions. Hence, EVs are a unique source of biomarkers, therapeutics, and theranostics, as their content is stabilized and protected against enzymatic degradation. They are biocompatible and permeable to biological barriers, have low toxicity and low immunogenicity, can be loaded with specific signaling molecules, and may be reengineered to express specific surface molecules, conveying EV-targeting capabilities to cells bearing cognate receptors (*11*).

Fetal-derived EVs (including placental) have recently been successfully isolated, sparking interest in uncovering their clinical implications (*13*, *14*). Multiple studies have linked fluctuations in maternal and fetal EV levels and their constituents to complications, such as GDM and PE (*13*, *15*). In addition, EVs have been recognized as

[1]Translational Extracellular Vesicles in Obstetrics and Gynae-Oncology Group, University of Queensland Centre for Clinical Research, Faculty of Medicine, Royal Brisbane and Women's Hospital, The University of Queensland, Herston, QLD 4006, Australia. [2]UQ Centre for Extracellular Vesicle Nanomedicine, Faculty of Medicine, The University of Queensland, Herston, QLD 4006, Australia. [3]Australian Institute for Bioengineering and Nanotechnology (AIBN), The University of Queensland, Brisbane, QLD 4072, Australia. [4]Department of Obstetrics and Gynecology, Maternal-Fetal Medicine, Ochsner Clinic Foundation, New Orleans, LA 70115, USA. [5]Department of Pharmacology, Faculty of Biological Sciences, University of Concepción, Concepción 160C, Chile. [6]School of Mechanical and Mining Engineering, Faculty of Engineering, Architecture, and Information Technology (EAIT), The University of Queensland, Brisbane, QLD 4072, Australia. [7]Departamento de Investigación, Postgrado y Educación Continua (DIPEC), Facultad de Ciencias de la Salud, Universidad del Alba, Santiago 8320000, Chile. [8]Mater Research, Faculty of Medicine, University of Queensland, Mater Health, South Brisbane 4101, Australia. [9]Department of Clinical Biochemistry, Aalborg University Hospital, Aalborg 9220 , Denmark. [10]Department of Materials Process Engineering Graduate School of Engineering, Nagoya University, Nagoya 464-8603, Japan.
*Corresponding author. Email: c.salomongallo@uq.edu.au (C.S.); y.yamauchi@uq.edu.au (Y.Y.)
†These authors contributed equally to this work.

messengers and significant contributors to viral infections during pregnancy and congenital anomalies (*16*). EVs can be detected within the maternal blood during the first trimester, with levels escalating as pregnancy advances, effectively serving as liquid biopsies that provide insights into the fetoplacental unit (*13*). Nevertheless, their low buoyant density, small size, and heterogeneity impede EV isolation from bodily fluids and their subsequent evaluation (*12*). Now used techniques for EV isolation, such as differential centrifugation and commercially available isolation kits, require numerous preparation steps involving ultracentrifugation and incubation phases that can require several hours. Alternatively, polymer-based precipitation offers a relatively simplified isolation approach that does not require ultracentrifugation or filtration. However, it requires optimized overnight incubation and is plagued by reduced specificity due to the concurrent isolation of contaminants and polymer molecules. Immunoaffinity isolation methods have recently gained traction as valuable tools for isolating EVs of specific origins. However, the efficacy of this approach hinges on the accurate screening of EV membrane markers, subsequent antibody-EV interactions, and ultimately elution buffer conditioning: pH, reducing agents, or detergents could potentially disrupt EV membrane permeability (*17*).

The emergence of nanotechnology and the evolution of nanoarchitectonics have improved EV isolation and detection (*18*). Superparamagnetic nanostructures for developing detection tools have become particularly important (*18*). We pioneered the development of mesoporous superparamagnetic nanostructures that specifically bind target biomolecules for specific and rapid isolation and to obtain target-specific signals. The associated porous structures provide a surface and interfacial bio-affinity that supports efficient analyte binding (*19*, *20*). Previously, we demonstrated that specially designed superparamagnetic gold–loaded ferric oxide nanocubes can isolate placental alkaline phosphatase (PLAP)–specific EVs within 4 hours, followed by a 1-hour colorimetric and electrochemical detection step (*21*). The nanocubes have a highly porous structure (i.e., a large surface area), making them useful for immobilizing many capture antibodies on their surface. However, this strategy requires long procedures, which is unsuitable for on-site screening of EV-like nanoparticles. Therefore, nanostructures that enable faster EV isolation and detection are needed for disease screening, which was the focus of the current study.

In this study, functionalized superparamagnetic mesoporous flower-shaped nickel ferrite spheres (SMNFs) are applied to develop a rapid and highly sensitive screening sensor for pregnancy complications based on placental EV detection. This system can readily analyze disease biomarkers and has the potential to be translated into clinical practice. This platform provides higher-performance, single-modality screening for early pregnancy complications that may be implemented within routine pathology.

RESULTS

Characteristics of the study population

A total of 201 pregnant women at early gestation (average 92 ± 13 days) were enrolled in this study (Fig. 1), of whom 101 were categorized as having a normal pregnancy and 100 were diagnosed with pregnancy complications, including GDM ($n = 28$), PE ($n = 23$), preterm birth (PTB; $n = 10$), and others ($n = 39$). The clinical characteristics of the pregnant females are presented in Table 1.

EVs were extracted from maternal plasma samples using a high-performance liquid chromatography (HPLC) system coupled with a size exclusion chromatography column. EVs were characterized by size, morphology, and phenotype using nanoparticle tracking analysis (NTA), cryo–transmission electron microscopy (cryo-TEM), and fluorescence imaging of single-particle interferometry (fig. S1). EVs had a size distribution of ~100 nm (mean, 105 ± 35 nm; fig. S1A), had a circular morphology with a lipid bilayer membrane observed by cryo-TEM (fig. S1B), and were positive for CD63, CD81, and CD9 (fig. S1C).

Cases and controls were randomly divided into the discovery/training groups (70%; $n = 71$ controls and $n = 70$ cases) and test (30%; $n = 30$ controls and $n = 30$ cases) cohorts (table S1). The discovery/training and test cohorts were matched by the gestational age at blood draw (case range, 65 to 130 days; and control range, 73 to 129 weeks). No significant differences ($P > 0.05$) were observed in gestational age, maternal weight, maternal height, maternal body mass index (BMI), birth weight, birth length (centimeters), head circumference (centimeters), or APGAR score between the cases and controls (tables S1 to S3).

Building a prediction model based on circulating placental extracellular vesicles for early identification of women at risk of pregnancy complication

Optimization of the predictive model

To ensure that the differences observed in biomarker performance were driven primarily by disease condition and not by variations in clinical characteristics, the biomarker workflow was adjusted according to BMI and ethnicity. This adjustment helped control for potential confounding factors, such as differences in maternal age and BMI, which could influence biomarker levels and classification efficiency. Controlling for these variables enhanced the specificity and accuracy of the predictive algorithms. This also strengthened the generalizability of the findings as it reduced the risk of bias and improved the reliability of biomarker performance across diverse patient populations.

Another important quality control measure implemented was the block randomization of samples during biomarker quantification. Block randomization is crucial to minimize potential batch effects and ensure that variations in biomarker measurements are not influenced by systematic biases introduced during the quantification process. This process involves grouping samples into randomized blocks before analysis, helping to evenly distribute any potential sources of experimental variability across the case and control samples. In biomarker studies, unaccounted variations in sample processing can produce misleading results by artificially inflating or deflating the biomarker levels. This method ensured that the observed differences in biomarker levels were due to biological factors rather than procedural inconsistencies, increasing the confidence in the model's predictive accuracy. Ultimately, block randomization strengthens the model by enhancing its reliability and reproducibility, supporting its application in diverse clinical settings.

Designing the model

A liquid chromatography–multiple reaction monitoring (LC-MRM) approach was designed to target the placental and EV-associated proteins PLAP, CD63, CD9, CD81, and tumor susceptibility gene 101 (TSG101) (Fig. 2). PLAP is expressed by trophoblast cells in the placenta, and PLAP-positive EVs increase in maternal blood throughout gestation (*13*, *22*). Several studies have linked $PLAP^+$

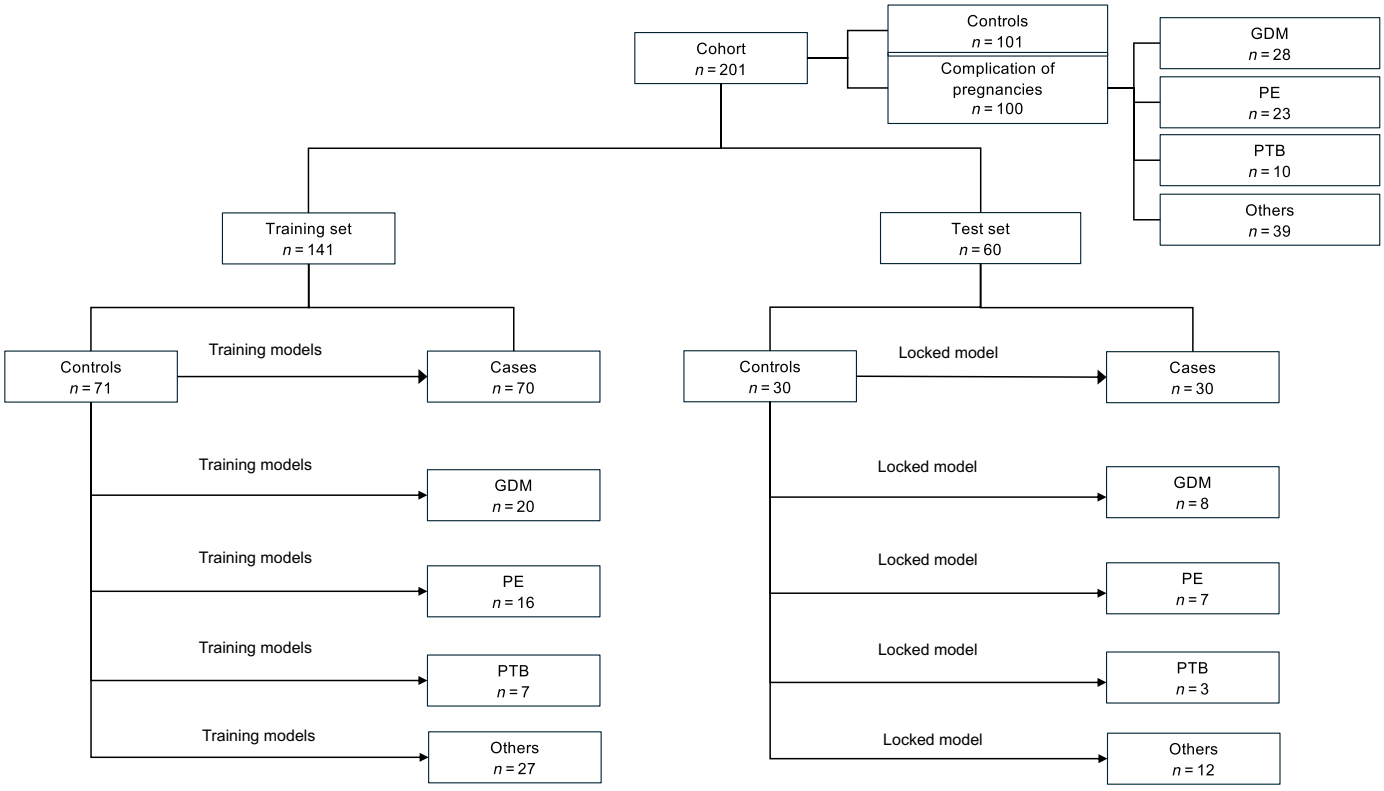

Fig. 1. Study population characteristics. A total of 201 pregnant women at early gestation were enrolled. For biomarker discovery and training, 141 women were included, with 71 controls (normal pregnancies) and 70 cases with pregnancy complications, specifically gestational diabetes mellitus (GDM; $n = 20$), preeclampsia (PE; $n = 16$), preterm birth (PTB; $n = 7$), and others ($n = 27$). The test set included 60 women, with 30 controls and 30 cases comprising GDM ($n = 8$), PE ($n = 7$), PTB ($n = 3$), and others ($n = 12$).

Table 1. Study participant demographics and clinical characteristics used in the training and test development.

	Training			Test			Training vs. test
		Control vs. case			Control vs. case		Control vs. case
	Control	Case	*P* value	Control	Case	*P* value	*P* value
Total *n*	71	70	–	30	30	–	–
Fetal sex						–	–
Female	36	35	–	16	14	–	–
Male	35	35	–	14	16	–	–
Clinical data (means ± SD)							
Gestational age (weeks)	13.0 ± 1.6	13.4 ± 2.0	0.17	13.2 ± 1.7	12.9 ± 2.0	0.91	0.70
Weight at collection (kg)	74.0 ± 21.0	76.9 ± 21.7	0.54	73.1 ± 21.9	77.2 ± 18.7	0.26	0.91
Height at collection (cm)	1.6 ± 0.1	1.6 ± 0.1	0.12	1.6 ± 0.1	1.6 ± 0.1	0.30	0.96
BMI at collection	27.9 ± 7.1	29.9 ± 11.4	0.43	27.9 ± 7.8	28.8 ± 6.6	0.52	0.93
Weight at birth (g)	3218.4 ± 471.7	3247.3 ± 492.7	0.50	3239.0 ± 388.3	3413.4 ± 581.1	0.54	0.47
Length at birth (cm)	50.3 ± 2.3	50.1 ± 2.3	0.64	50.1 ± 2.0	50.4 ± 2.2	0.66	0.85
Head circumference (cm)	33.9 ± 1.5	34.3 ± 1.4	0.09	33.1 ± 4.6	34.3 ± 1.6	0.51	0.82
APGAR score, 1 min	8.1 ± 1.5	8.2 ± 1.3	0.94	8.5 ± 1.0	8.2 ± 1.2	0.13	0.58

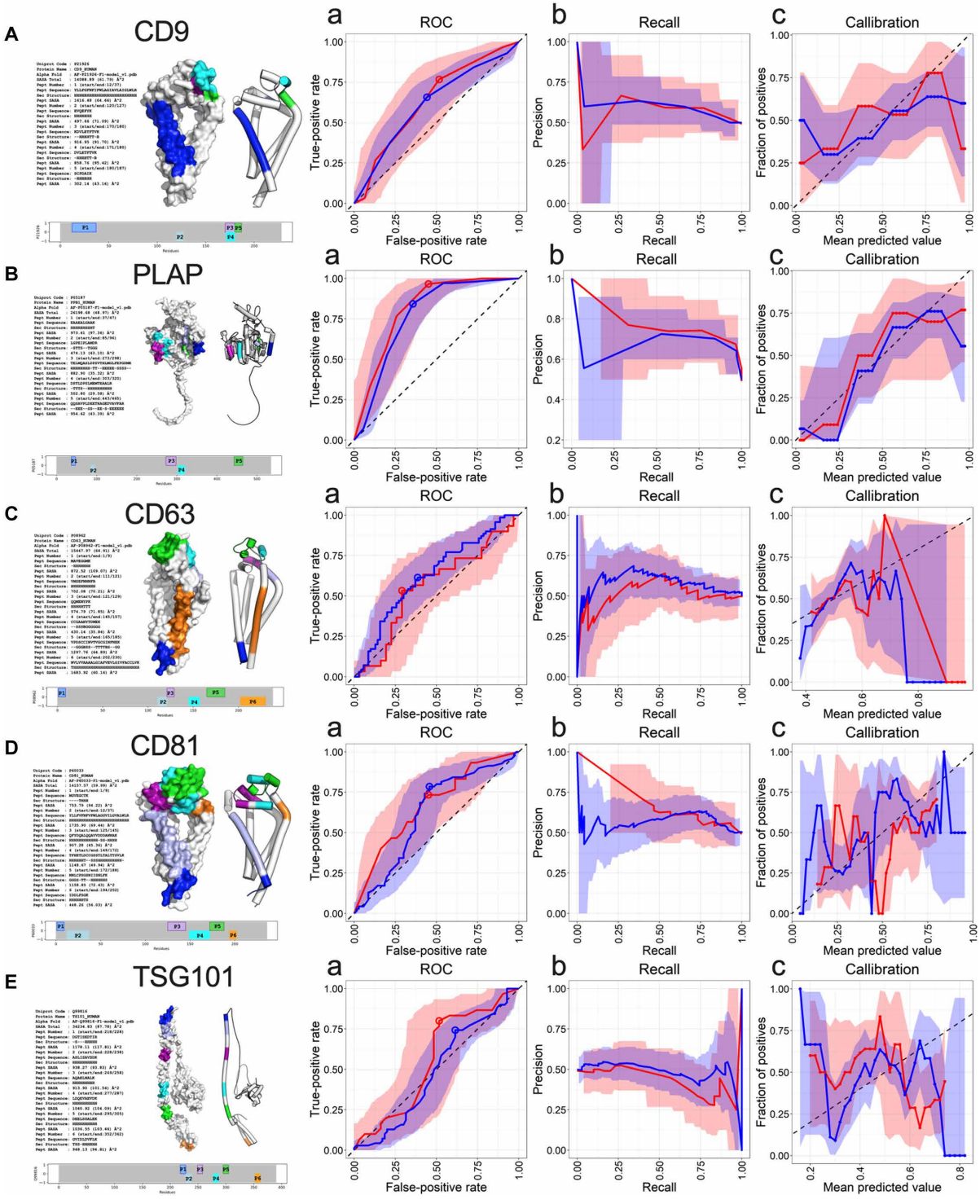

Fig. 2. Individual performance of proteins associated with EV and placenta in predicting the risk of pregnancy complications. (A to E) Peptides are colored for each protein structure based on the Protein Data Bank (PDB) with the best resolution and coverture available. The structures were prepared with PyMOL in surface mode, and biological assembly was available from PDB (monomer, dimer, and tetramer). (**A**) CD9, (**B**) PLAP, (**C**) CD63, (**D**) CD81, and (**E**) TSG101. a, area under the receiver operating characteristic curve (AUROC); b, area under the precision-recall curve (AUPRC); c, calibration curve. Data are presented as mean values generated via bootstrapping (discovery/training set, $n = 140$; and test set, $n = 70$) with a 95% confidence interval. Blue line, training set; red line, test set.

EVs to placental dysfunction and adverse pregnancy outcomes. The EV markers CD9, CD63, CD81, and TSG101 were selected on the basis of the International Society for Extracellular Vesicles guidelines, particularly the Minimal Information Available for Studies of Extracellular Vesicles 2018 (MISEV2018) and MISEV2023 recommendations, which identify CD9, CD63, and CD81 as key tetraspanins and TSG101 as an ESCRT (endosomal sorting complexes required for transport)–related protein associated with EVs (*17*, *23*). The PyCaret classification module was used to train 14 different algorithms for the two outcomes (case and control). A rigorous workflow was applied to develop a prediction model that included a comprehensive biomarker analysis with cross-validation to ensure generalizability. Using the randomly selected discovery/training set (70 cases and 71 controls), the model that best predicted the risk of pregnancy-related complications was identified. This model was then "locked" and evaluated on the independent test cohort (30 cases and 30 controls) using a 10-fold cross-validation strategy.

Using CD9 as a variable, the best model predicted 77 and 27 cases and 63 and 34 controls in the training and test cohorts, respectively. Of these, 46 of 77 (60%) and 16 of 27 (59%) of the predicted cases and 39 of 63 (62%) and 20 of 34 (59%) of the predicted controls were classified correctly (Fig. 2A). Moreover, the area under the receiver operating characteristic curve (AUROC) was 0.62/0.64 (Fig. 2Aa), and the area under the precision-recall curve (AUPRC) was 0.60/0.57 (Fig. 2Ab).

Using PLAP as a variable, the best model predicted 84 and 31 cases and 56 and 30 controls in the training and test cohorts, respectively. Of these, 59 of 84 (70%) and 23 of 31 (74%) of the predicted cases and 45 of 56 (80%) and 23 of 30 (77%) of the predicted controls were classified correctly (Fig. 2B); the AUROC was 0.77/0.81 (Fig. 2Ba), and the AUPRC was 0.68/0.78 (Fig. 2Bb).

Using CD63 as a variable, the best model predicted 49 and 24 cases and 91 and 37 controls in the training and test cohorts, respectively. Of these, 31 of 49 (63%) and 15 of 24 (63%) of the predicted cases and 52 of 91 (57%) and 22 of 37 (59%) of the predicted controls were classified correctly (Fig. 2C); the AUROC was 0.63/0.56 (Fig. 2Ca), and the AUPRC was 0.58/0.51 (Fig. 2Cb).

Using CD81 as a variable, the best model predicted 80 and 37 cases and 60 and 24 controls in the training and test cohorts, respectively. Of these, 50 of 80 (63%) and 22 of 37 (59%) of the predicted cases and 40 of 60 (67%) and 16 of 24 (67%) of the predicted controls were classified correctly (Fig. 2D); the AUROC was 0.62/0.67 (Fig. 2Da), and the AUPRC was 0.57/0.70 (Fig. 2Db).

Using TSG101 as a variable, the best model predicted 84 and 24 cases and 56 and 37 controls in the training and test cohorts, respectively. Of these, 44 of 84 (52%) and 8 of 24 (33%) of the predicted cases and 30 of 56 (54%) and 15 of 37 (41%) of the predicted controls were classified correctly (Fig. 2E); the AUROC was 0.48/0.56 (Fig. 2Ea), and the AUPRC was 0.54/0.61 (Fig. 2Eb).

The Brier score was calculated for each variable to assess the accuracy of the probabilistic predictions (table S4). The best predictions were obtained using PLAP, with a Brier score of 0.19 (Fig. 2, Ac to Ec). A comparison of biomarker analysis based on AUROC, precision/recall, and calibration between training and test data suggests that the model did not overfit the data. CD9, CD63, and CD81 showed consistent predictive performance; TSG101 exhibited poorer performance as a predictive marker in this specific context.

Next, the effect of combining all variables on the efficiency of the models to identify individuals most at risk of developing pregnancy complications was evaluated. Combining all variables improved the performance of each variable (AUROC, 0.90; AUPRC, 0.93; Brier score, 0.15; Fig. 3A, a to c) in the test cohort for predicting pregnancy complications. Based on the feature selection algorithm, the variables that contributed the most to performance were PLAP and CD9 (fig. S2). In particular, in the test cohort, the model demonstrated high accuracy in identifying individuals at early gestation who would develop GDM {accuracy, 97%; sensitivity, 100% [95% confidence interval (CI), 75 to 100%]; and specificity, 97% (95% CI, 90 to 100%); Fig. 3B, a to c}.

The model also effectively identified individuals at risk of PE (Fig. 3C), PTB (Fig. 3D), and other complications (Fig. 3E). For PE, the model achieved an optimal sensitivity of 100% (95% CI, 75 to 100%) and specificity of 97% (95% CI, 90 to 100%) with an overall accuracy of 92%. For PTB, the model had an optimal sensitivity of 67% (95% CI, 0 to 100%) and specificity of 97% (95% CI, 32 to 100%), with an overall accuracy of 94%. Last, for other pregnancy conditions—excluding GDM, PE, and PTB—the model had an optimal sensitivity of 75% (95% CI, 42 to 100%) and a specificity of 83% (95% CI, 50 to 100%), with an overall accuracy of 81%. The model performance was consistent between the training and test cohorts, indicating that the data were not overfitted.

While CD63, CD81, and TSG101 showed similar performances, combining PLAP and CD9 provided the most significant contribution to improving classification efficiency (fig. S2). Notably, when only PLAP and CD9 were included in the model, nearly identical classification efficiencies were achieved as when all biomarkers were incorporated. This indicated that PLAP and CD9 were the primary drivers of the classification model's predictive power.

Synthesis, characterization, and nanozyme activity of SMNFs

Although research on EVs has advanced significantly, the limited concentration of isolated EVs hampers their efficiency and precision, making their enrichment and purification crucial for subsequent analyses (*24*, *25*). Enrichment of EVs using magnetic beads has garnered increasing attention. Despite substantial progress, this method has notable limitations, such as the simple surface structure of conventional magnetic beads, few immobilized probes, and inefficient separation, even with complex surface modifications (*25*).

To develop a sensor to quantify the placental EVs present in the maternal circulation during gestation, SMNFs with multiple nanopetals were synthesized. These structures provide excellent structural stability and offer extraordinary surface functions, enabling efficient EV isolation and purification (*25*–*27*). SMNFs were synthesized using a solvothermal method combined with high-temperature calcination in air (fig. S3). Briefly, 0.5 mmol of $Fe(NO_3)_3{\cdot}9H_2O$ and 0.5 mmol of $Ni(NO_3)_3{\cdot}6H_2O$ were dissolved in 40 ml of isopropanol under vigorous stirring. After complete dissolution, 8 ml of glycerol was added, stirred, heated at 180°C, and centrifuged; the greenish precipitate (i.e., nickel-iron glycerate) was collected.

The as-prepared nickel-iron glycerate exhibited a spherical shape with an approximate size of 180 to 200 nm (fig. S4A). This intermediate complex may have contained C—O, C—H, and O—H bonds from the organic glycerol. These organic constituents were removed by calcination under an air atmosphere, and the nickel-iron glycerate precursor was converted into the iron oxide phase. The as-prepared dried nickel-iron glycerate was subsequently heated under an air atmosphere at 350°C for 2 hours at 1°C min^{-1}. The calcination

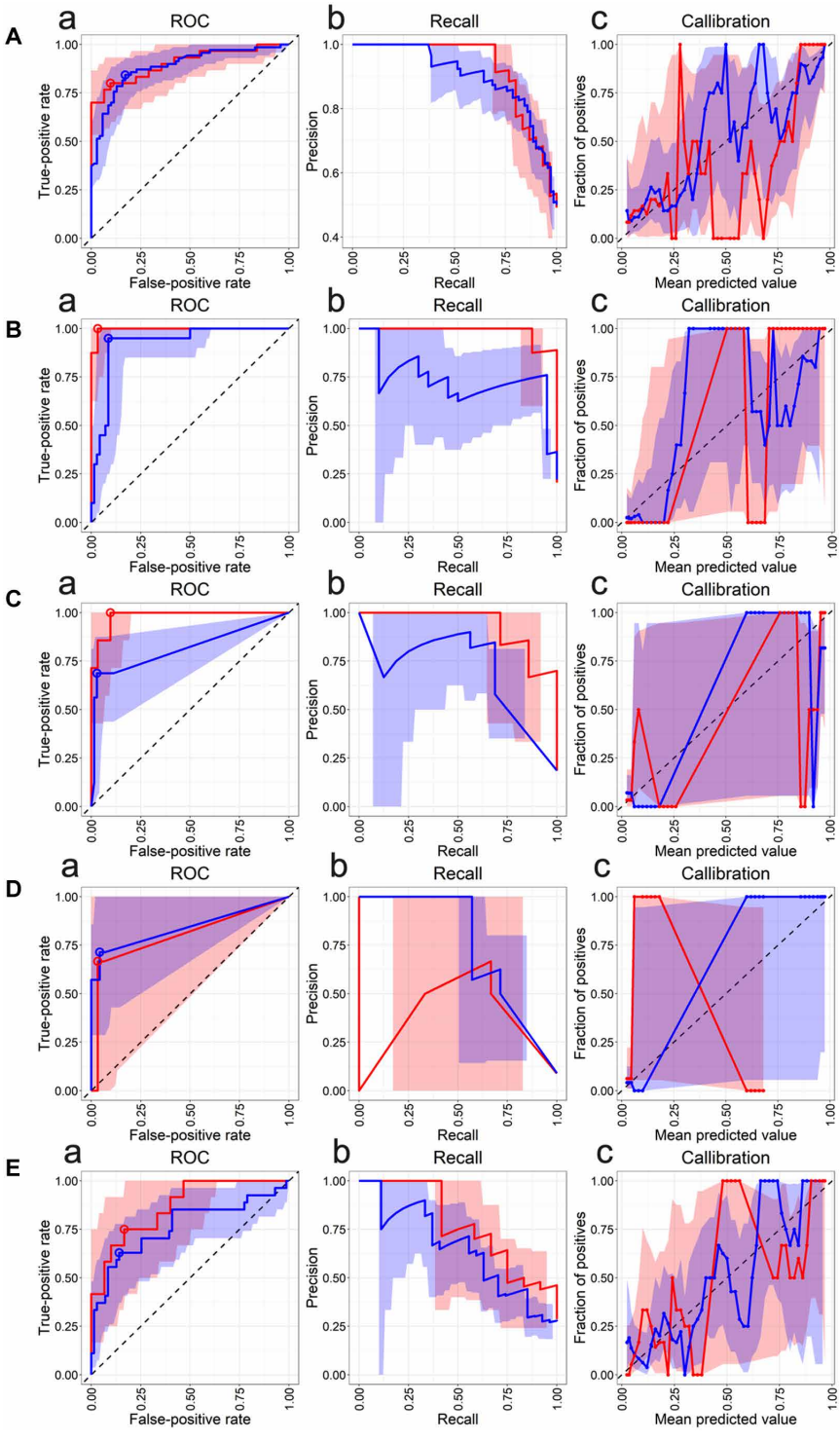

Fig. 3. Predictive model performance under combined CD9, PLAP, CD63, CD81, and TSG101EV. (**A**) Binominal model for cases of all pregnancy complications and controls. (**B**) Binominal model for cases of GDM and controls. (**C**) Binominal model for cases of PE and controls. (**D**) Binominal model for cases of PTB and controls. (**E**) Binominal model for cases of other complications (excluding GDM, PE, and PTB) and controls. a, AUROC; b, AUPRC; c, calibration curve. Data are presented as mean values generated via bootstrapping (discovery/training, $n = 140$; and test, $n = 70$) with a 95% confidence interval. Blue line, training set; red line, test set.

process removed the organic glycerate constituents and yielded 100- to 120-nm SMNFs (fig. S4B). The compositions of the products were analyzed using x-ray photoelectron spectroscopy (XPS) (fig. S5). The survey spectrum of the SMNFs (fig. S5A) confirmed the presence of Fe, Ni, and O. The high-resolution XPS spectrum of Fe 2p revealed two major peaks, corresponding to Fe^{2+} and Fe^{3+}, respectively, along with satellite peaks. This indicates that iron in the SMNFs exists in both Fe^{2+} and Fe^{3+} states (fig. S5B). In addition, Ni was identified as a mixture of Ni^{2+} and Ni^{3+} oxidation states (*27*). The coexistence of Ni^{2+}, Ni^{3+}, Fe^{2+}, and Fe^{3+} was a common characteristic of nickel-doped ferrite structures (*27*). An XRD analysis was performed to investigate the purity and phase composition of the SMNFs (fig. S6), revealing no impurities (JCPDS, no. 54-0964). Superparamagnetic nanomaterials are crucial for magnet-based pre-concentration, isolation, separation, and purification of target analytes from complex biological systems. These nanomaterials exhibited no net magnetic moment without an external magnetic field but aligned their magnetic moments when a field was applied, reverting to a nonmagnetic state once the field was removed. This property enabled the precise magnetic manipulation of samples for the specific and sensitive detection of target molecules (*28*–*30*). The SMNFs demonstrated complete reversibility of the M-H curve across temperatures from 5 to 300 K. The S-shaped hysteresis loops shown in fig. S7, with a negligible coercive field (H_c), are indicative of the superparamagnetic nature of the SMNFs.

Nanozymes are increasingly favored in biosensing for their enzymatic mimicry, stability, and cost-effective synthesis, enabling rapid and affordable point-of-care applications (*31*, *32*). Herein, to assess the peroxidase-mimicking activity of the as-synthesized SMNFs, several control experiments were performed. In the positive test sample, SMNFs were incubated with the freshly prepared 3,3′,5,5′-tetramethylbenzidine (TMB) substrate solution; the negative control did not have SMNFs. After incubation, a clear blue solution was observed for the positive sample, whereas the negative sample was colorless. The absorbance of the positive sample was ~18 times higher than that of the negative control (0.85 versus 0.047; fig. S8).

The amount of SMNFs and the substrate solution pH were optimized to achieve the optimal peroxidase-like activity. The highest responses in colorimetry and amperometric readouts were obtained at pH 2.5 (fig. S9A). However, considering that iron can leach from the SMNFs at pH < 3.0, pH 3.5 was selected for subsequent experiments. In addition, 5 and 10 μg of SMNFs produced similar responses (fig. S9B); therefore, 5 μg was selected as the optimal amount.

In the following assays, the SMNFs were functionalized with target-specific antibodies, which could affect the nanozyme activity by covering the active sites. Hence, the nanozyme activity of the SMNFs was analyzed after antibody functionalization. As expected, a reduction in absorbance occurred (fig. S10). However, the nanozyme response remained sufficiently high for the sensor design.

The steady-state kinetics of peroxidase mimetics was evaluated by varying the concentrations of TMB (0.01 to 0.9 mM) and H_2O_2 (0.01 to 1.0 M) at a constant H_2O_2 (500 mM) and TMB (700 μM) concentration, respectively (fig. S11). The Michaelis constant (K_m) and maximum rate of reaction (V_{max}) values were estimated using the Lineweaver-Burk and Michaelis-Menten equations. The K_m values for TMB and H_2O_2 were 0.129 and 138.5 mM, respectively (fig. S11), markedly superior to those recently reported for nanomaterial-based nanozymes. This enhancement is likely due to the three-dimensional nanopetals creating unique diffusional environments and exposing the Fe active sites. In addition, while most reported nanozymes exhibit high activity at elevated temperatures or require active site modifications using complex chemistry (*33*, *34*), the current study's nanozyme demonstrated high activity at room temperature without additional chemical modifications. This functionality provides a unique opportunity for advancing nanozyme-based biosensing, particularly for devices intended for use in resource-limited settings.

SMNF-based magnetic isolation and 4-flex readout system for EVs

Placental small EVs (sEVs) can be detected in the maternal circulation as early as 6 weeks of gestation (*35*); placental sEVs constitute ~20% of the total sEVs in the maternal circulation at term (*36*). However, circulating sEVs (total and placenta-derived) are higher throughout pregnancy in individuals with GDM than in those with normal pregnancies (*13*), suggesting that EVs may be used as biomarkers for GDM. However, challenges in biomarker identification and validation, sensitivity and specificity, sample preparation, and stability must be addressed to ensure the effectiveness and reliability of biomarkers in clinical settings.

PLAP and CD9 antibodies were incorporated into the prediction model for the early identification of individuals at risk of developing pregnancy complications based on their strong individual performance. In this assay, the SMNFs were functionalized with anti-PLAP antibodies to specifically isolate $PLAP^+$ EVs using a simple magnet (Fig. 4A). The magnetically isolated SMNF-EV complexes were incubated on a 4-flex glass strip pre-functionalized with anti-CD9 (Fig. 4B). The 4-flex glass sensor provided high specificity for targeted EVs along with three controls, enabling easy and single-step screening.

To evaluate the capability of the antibodies to create an efficient and sensitive assay on glass, SMNFs were functionalized with different antibodies. The antibodies were attached to the SMNFs surface using 1-ethyl-3-(3-dimethylaminopropyl)carbodiimide/*N*-hydroxysuccinimide (EDC-NHS) coupling chemistry, followed by streptavidin modification, allowing biotinylated antibodies to easily attach via avidin-biotin coupling. The PLAP/SMNFs were incubated in the cell culture medium collected from a placental choriocarcinoma cell (BeWo) culture, and subsequent assays were performed on the anti-CD9 functionalized glass surface. CD9 nonspecifically isolated significantly more EVs than anti-8B6, monoclonal immunoglobulin G (IgG), and polyclonal IgG (Fig. 4C). The anti-PLAP antibody isolated PLAP-specific EVs from BeWo cells, with a lower response observed in a human trophoblast cell line (HTR-8 cells).

In addition, the SMNF-isolated EV fraction and the non–PLAP-specific EV fraction were evaluated. The SMNF-EV fraction showed a much higher response (>19 times higher) than the non–PLAP-specific fraction; within 30 min, the PLAP-SMNF system isolated the maximum amount of $PLAP(^+)$ EVs (Fig. 4D). These results were confirmed via NTA measurements (Fig. 4E). These results demonstrate the high efficiency of an SMNF-based system for isolating EVs from cell culture medium.

A set of control experiments was conducted to verify the assay specificity and sensor functionality using an anti-PLAP antibody. In the positive control experiments, PLAP-functionalized SMNFs were initially incubated in BeWo cell culture medium and then subpopulated with anti-CD9 antibodies immobilized onto the

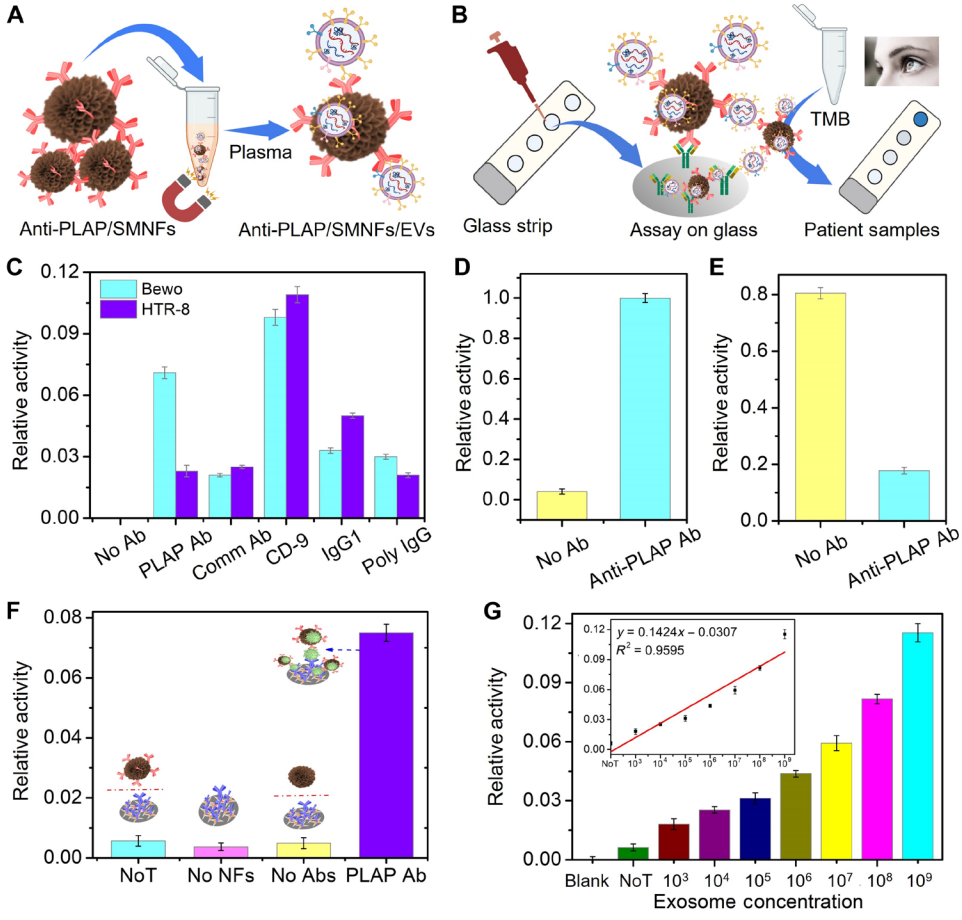

Fig. 4. SMNF-based 4-flex glass nanosensor for PLAP$^+$ EVs isolation and detection. (**A**) Direct isolation of PLAP$^+$ EVs using anti-PLAP modified SMNFs; (**B**) schematic representation of the assay on the 4-flex glass sensor; (**C**) relative activity of the assay with different types of antibodies obtained from BeWo and HTR-8 cell lines; (**D**) relative activity of assay with no antibody or with a PLAP antibody; (**E**) NTA responses after isolating EVs using unmodified SMNFs and anti-PLAP modified SMNFs; (**F**) responses of the assay for target samples against three controls [no-target (NoT): EV sample is replaced by PBS; No SMNFs: EVs are not extracted by PLAP modified SMNFs; No Abs: SMNFs are not modified with PLAP antibody (Ab)]; (**G**) relative activity (absorbance at 652 nm) for the designated concentration of exosomes extracted from a GDM (BeWo) cell line. The concentration varies between 10^3 and 10^9 particles/ml, equivalent to 8×10^6 versus 8×10^{11} vesicles per million cells/24 hours.

streptavidin-modified glass substrate. A significant amount of activity (0.8125) was observed for placental choriocarcinoma–derived EVs (Fig. 4F). In addition, no-target control experiments were performed using phosphate-buffered saline (PBS) instead of BeWo-derived cell culture medium. As expected, a low response rate (0.057) was observed. Similarly, the control experiment without PLAP-SMNFs exhibited a negligible response (0.051). These control experiments demonstrated the high specificity of the assay for isolating and detecting PLAP$^+$ EVs in cell culture medium, exhibiting negligible background interference.

To determine the sensitivity of the detection system, a designated concentration of exosomes (10^3 to 10^9 equivalent to 8×10^6 to 8×10^{12} EVs per million cells/24 hours) from BeWo cell lines was prepared by serial dilution. The response (colorimetric) increased with increasing concentrations of target EVs (Fig. 4G). The higher abundance of target EVs was attributed to the increased amount of SMNFs on the glass surface, which increased the SMNFs' nanozyme-mediated oxidation of TMB, resulting in enhanced color responses. The linear regression equation was $y = 0.1424x - 0.0307$, with a coefficient of determination (R^2) of 0.9595 and a limit of detection of 10^3 EVs per million cells/24 hours. The relative SD (% RSD) of the three independent measurements was <6.0%, suggesting good reproducibility of the nanosensor. This detection limit is 10^4-fold higher than conventional techniques, such as enzyme-linked immunosorbent assay (10^3 EVs/ml versus 10^7 EVs/ml per million cells/24 hours). The assay demonstrated nearly 10 times higher sensitivity (8×10^6 versus 8.7×10^7 vesicles per million cells/24 hours) than NTA in fluorescence mode (*21*).

Sensor performance in clinical samples

The model has a high sensitivity and specificity for identifying pregnant females at risk of later GDM diagnosis. The classification efficiency for GDM remained consistent between the discovery/training and test cohorts, demonstrating high reproducibility without a decrease in performance metrics (table S2). These findings suggest that the CD9/PLAP biomarker panel is particularly robust for GDM risk assessment. Hence, the CD9$^+$/PLAP$^+$ sensor system was validated using plasma samples from the GDM cohort (table S5). Placental EVs were quantified in the plasma, and EVs were extracted using matched samples (Fig. 5). No difference was

identified between the quantification of $CD9^+/PLAP^+$ in EV and plasma samples for GDM (Fig. 5A) or healthy controls (Fig. 5B). In addition, comparative analysis of placental $CD9^+/PLAP^+$ EVs (Fig. 5C) and plasma samples (Fig. 5D) detected using the sensor showed higher levels in GDM individuals than controls. Hence, plasma measurements alone may be sufficient for early detection of GDM, simplifying the diagnostic process. These data suggest the potential utility of the $CD9^+/PLAP^+$ sensor system as a noninvasive and reliable method for the early identification of women who will develop GDM.

The sensor's performance for detecting $CD9^+/PLAP^+$ placental EVs in plasma compared to extracted EVs was evaluated by applying the biomarker workflow. The best-performing model applied linear discriminant analysis and used the quantification of placental EV as the input with 10-fold cross-validation. Using plasma, the model predicted 100 and 100% of the predicted cases and 89 and 92% of the predicted controls in the training and test sets, respectively. The model had an AUROC of 0.98 (Fig. 6Aa), AUPRC of 0.99 (Fig. 6Ab), and a Brier score of 0.07 in the test set (Fig. 6Ac). Using the extracted EVs, the model correctly predicted 40 and 100% of the predicted cases and 40 and 100% of the predicted controls in the training and test sets, respectively. The model had an AUROC of 1.0 (Fig. 6Ba), AUPRC of 1.0 (Fig. 6Bb), and a Brier score of 0.01 in the test set (Fig. 6Bc; table S6). These data demonstrate that quantifying placental EVs ($CD9^+/PLAP^+$) can be a reliable early biomarker to identify individuals at risk of developing GDM, with extracted EVs showing superior performance to plasma. However, plasma and extracted EVs had accuracies exceeding 90%.

GDM is associated with impaired glucose metabolism in the first trimester of pregnancy; several studies have evaluated the ability of plasma glucose or glycosylated hemoglobin (HbA1c) to predict early GDM (*37*–*40*). Hence, the biomarker performance of fasting blood glucose levels during early gestation was evaluated to predict GDM development at 22 to 28 weeks of gestation. Fasting glucose levels measured in early gestation predicted the development of GDM, with an overall performance of 0.56 [area under the curve (AUC)], sensitivity of 58%, and specificity of 54% (fig. S12). In contrast, the performance of PLAP/CD9 as biomarkers was significantly higher, offering improved sensitivity and specificity for identifying women at risk of developing GDM. These findings highlight the potential of PLAP/CD9-based biomarkers to surpass traditional indicators, such as fasting glucose, in terms of predictive accuracy, particularly for early detection of GDM. Given the limitations of fasting glucose and HbA1c levels in identifying GDM risk early in pregnancy, PLAP/CD9 biomarkers may be more effective for timely intervention and monitoring.

The accuracy, sensitivity, and specificity of fasting glucose levels measured between 11 and 13 weeks of gestation for predicting GDM development between 22 and 28 weeks have been evaluated previously; however, the values can vary depending on the population and specific cutoff values (*38*, *41*, *42*). Although fasting glucose levels in the first trimester have been associated with the development of GDM, they lack sufficient sensitivity and specificity to be the sole predictor (*38*, *40*, *41*). Combining fasting glucose with other biomarkers or clinical risk factors tends to improve predictive performance, making the identification of women at risk of GDM more reliable.

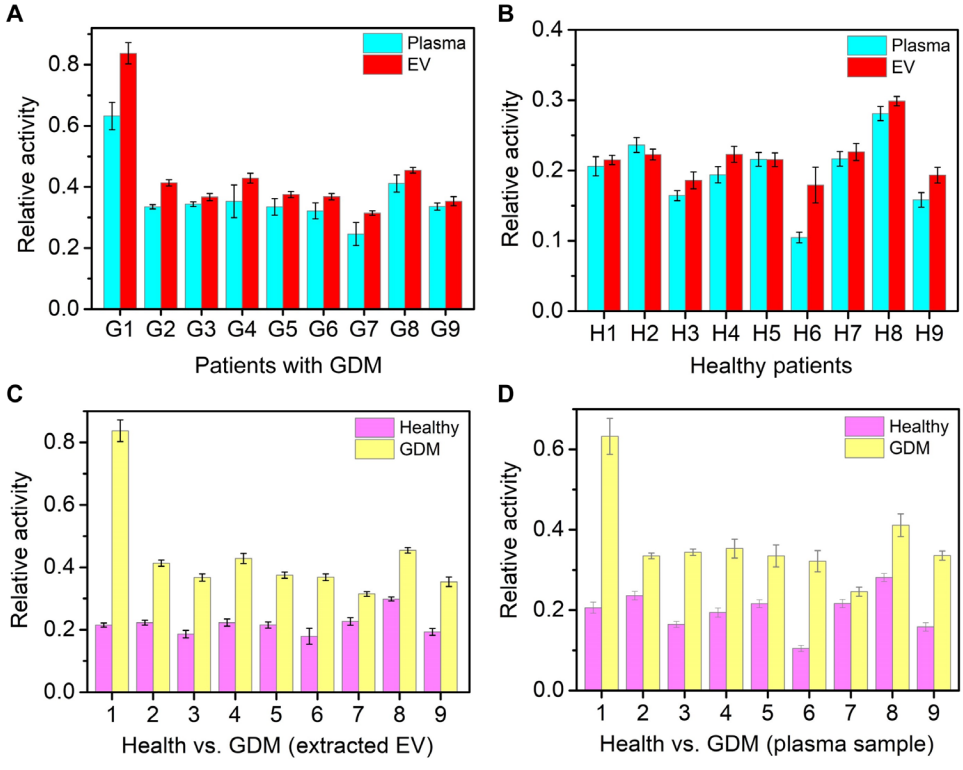

Fig. 5. Patient sample analysis. Relative activity of plasma and extract EV samples from (**A**) patients with GDM and (**B**) healthy patients; side-by-side comparison of responses obtained from (**C**) extracted EVs and (**D**) plasma samples.

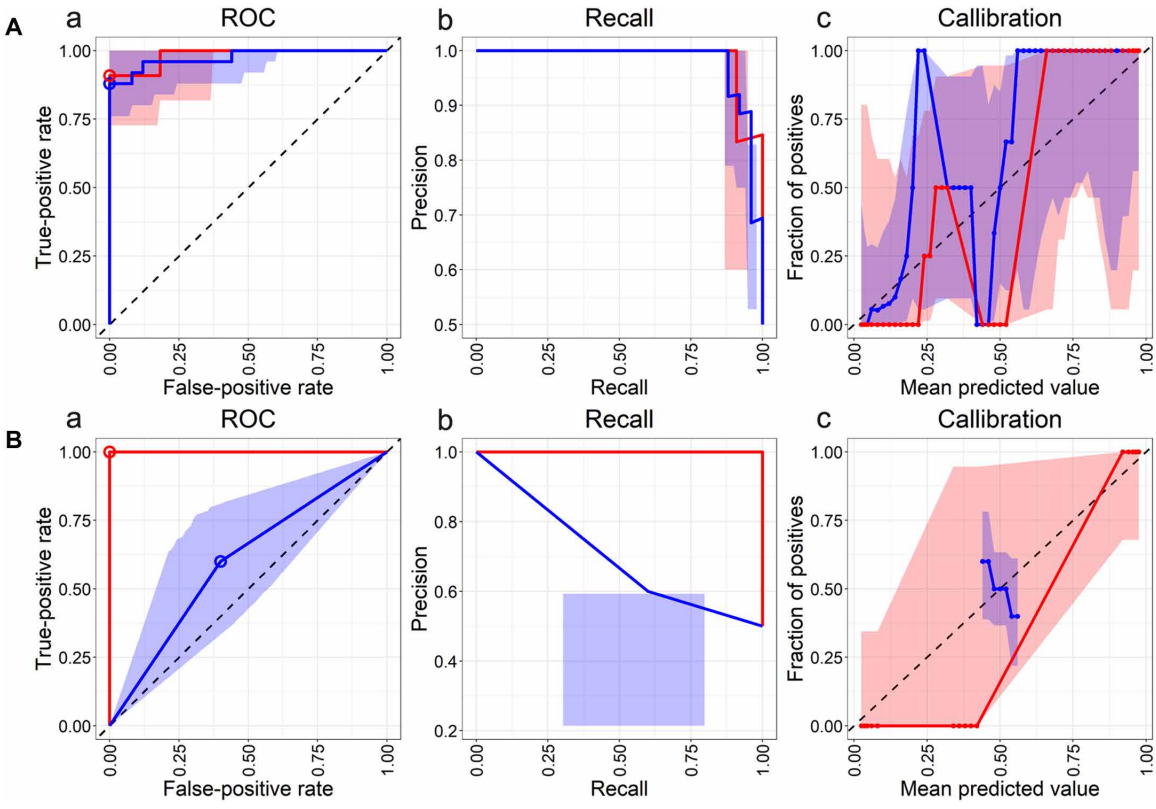

Fig. 6. Predictive performance of the sensor to identify individuals at risk of developing GDM. (**A**) Plasma samples; (**B**) extracted EVs; a, AUROC; b, AUPRC; c, calibration curve. Data are presented as mean values generated via bootstrapping with a 95% confidence interval. Blue line, training set; red line, test set.

DISCUSSION

In this study, a rapid sensor was developed and optimized to quantify placental EVs, and its ability to identify individuals at risk of developing GDM was validated, specifically for use in the first trimester of pregnancy. More specifically, a targeted proteomics approach was adopted to identify and validate a set of peptides that could quantify circulating placental EVs in maternal plasma during early gestation. These peptides effectively identified the early risks of different pregnancy complications in the discovery and verification cohorts of pregnant women. Consistent with previous studies that focused on profiling EVs throughout pregnancy and early pregnancy risk prediction, the specific peptides of the key proteins associated with extracellular vesicles (i.e., CD9, CD63, CD81, and TSG101) and placental tissue (i.e., PLAP) were verified. The quantification of placental EV biomarkers differentiated cases (patients who developed pregnancy complications) and controls (those who did not) and distinguished different categories of pregnancy-related complications, including GDM, PE, and PTB.

Using MRM, the tetraspanin CD9 and PLAP proteins were analyzed within circulating EVs from maternal plasma collected during early gestation. This approach identified a distinct pattern of expression that could effectively distinguish between individuals at early gestation most likely to develop GDM and those with a normal pregnancy, achieving a combined sensitivity (i.e., using plasma or extracted EVs) of 95%, specificity of 100%, positive predictive value (PPV) of 100% (95% CI, 100 to 100%), and negative predictive value (NPV) of 96% (95% CI, 89 to 100%). Furthermore, quantifying PLAP/CD9 in EVs or whole plasma (without EV isolation) yielded a similar classification efficiency for identifying patients at risk of developing GDM. Hence, isolating EVs may not be necessary to yield accurate results and simplify the workflow. Using whole plasma directly would facilitate clinical implementation by making the test more compatible with routine laboratory pathology procedures, potentially lowering costs, reducing processing time, and improving sample consistency.

The concentration of circulating EVs, including those expressing CD9 and PLAP, is significantly higher in pregnant than nonpregnant women (*43*). This increase is primarily attributed to the release of EVs of placental origin (*44*). Moreover, during a healthy pregnancy, the number of EVs in the maternal plasma continues to increase with gestational age, increasing by more than twofold as pregnancy progresses (*13*). This likely reflects the growing metabolic and immunological demands of the developing fetus and placenta, highlighting the importance of EVs as regulators of immune modulation, nutrient transport, and signaling between the mother and fetus (*45*). These gestational age-dependent increases in the number of CD9- and PLAP-positive EVs underscore their potential as biomarkers for monitoring and assessing the health and progression of pregnancy.

Alterations in the concentration and content of circulating placental EVs in maternal blood are characteristic of various pregnancy complications, including GDM, PE, fetal growth restriction, and PTB (*13*, *46*–*48*). These complications often share a common physiological

placental dysfunction pathway, which can disrupt the normal signaling processes between the mother and fetus. This disruption is reflected in changes in the quantity and molecular content of EVs released from the placenta early in pregnancy, potentially serving as an early indicator of a mother's susceptibility to developing complications later in gestation (*49*–*51*). Thus, although each pregnancy complication has distinct clinical features, they may share early EV biomarker signatures due to similar underlying placental stress or dysfunction. Future studies investigating the specific molecular mechanisms and pathways driving EV changes under different conditions would be valuable for refining disease-specific biomarkers.

In the current study, Ni-ferrite–based SMNFs with multiple nanopetals were designed to achieve portability, high specificity, and high detection sensitivity. These SMNFs act as nanovehicles to directly isolate target EVs expressing CD9 and PLAP and function as nanozymes. Accordingly, this system was combined with a sensitive and robust nanozyme-based readout system on a 4-flex glass strip. The SMNFs isolated the target EVs within 30 min, followed by assay formation and nanozymatic readout within another 30 min. The 4-flex system allows the comparison of target signals with triple-negative controls, demonstrating the high specificity of the detection system. The SMNFs showed high enzyme-like activity even at room temperature, enabling highly sensitive detection of EVs (1000 EVs per million cells/24 hours). The performance of the SMNFs nanosensor is comparable to or surpasses that of recently reported nanostructure-based EVs. For example, Yokoi *et al.* (*52*) used polyketone nanowires with ZnO nanowires to identify high-grade serous ovarian cancer, which requires further ketonic modifications. In another study, magnetic nanomaterials required conjugation with $MgSiO_3$ to achieve high isolation capability (*53*). However, neither strategy integrates isolation and detection using separate materials or strategies. In contrast, the nanosensor described in the current study uses nanostructured SMNFs that do not require complex functionalization or the formation of intricate nanomaterials. In this way, the nanoengineered SMNFs perform isolation and readout of the target EVs.

This 4-flex sensor boasts certain key advantages. (i) It can be exploited as a rapid first-pass screening (yes/no) tool to detect pregnancy complications. (ii) This platform does not require expensive total exosome isolation, which is a time-consuming and laborious step. Using SMNFs as nanovehicles to directly isolate EVs reduces the number of steps requiring expensive reagents and sophisticated instruments. (iii) The readout system is based on the nanozyme activity of SMNFs; that is, a single nanomaterial performs the isolation and detection steps, further reducing the expenses and improving portability. This assay also replaces natural enzymes with chromogenic substances (e.g., TMB oxidation), reducing the cost, handling, and storage facilities generally required for natural enzymes. (iv) The nanosensor has a target chamber and three controls, confirming its high specificity. (v) The PLAP-SMNFs are highly stable and remain dispersed for an extended period; therefore, once prepared, they can be used for multiple analyses. Once PLAP and 4-flex functionalization occur, they can be stored and used to analyze at least three patient samples.

The sample size is critical to ensuring that the results are representative of the general population, particularly given the varying incidences of pregnancy complications. Accordingly, a power calculation was performed for each biomarker to determine the ability to detect statistically significant differences with high confidence (table S7). By achieving sufficient statistical power, the risk of false negatives was minimized. The study sample size was, therefore, sufficient to detect the observed differences across biomarkers, enhancing the study's robustness. While the AUC value of 1.0 in the training set suggested excellent predictive performance, the AUC of 0.9 in the test cohort might better reflect the general population. The candidate biomarkers identified in this cohort should be confirmed in a larger multicenter, independent cohort. Moreover, future validation studies are required to establish the clinical utility of this approach for the early diagnosis and prognosis of GDM in obstetrical triage settings and to better define the performance limits of the approach regarding factors such as the interval from blood draw to GDM diagnosis.

Overall, this innovative platform uses EVs to identify individuals at risk of developing GDM at an early stage of pregnancy with a classification accuracy of >90%. This approach has significant potential for clinical application and offers an effective tool for early diagnosis and intervention. Moreover, it is relatively inexpensive, portable, and adaptable for detecting other targeted EVs. Hence, it can be readily developed into a simple yet high-performance screening tool for pregnancy complications in point-of-care settings.

MATERIALS AND METHODS

Sample collection

A case-control study design was used to establish pregnancy-associated changes in placental EVs in maternal plasma obtained from normal pregnant females and those with pregnancy complications. The human plasma samples were obtained in accordance with the principles of the Declaration of Helsinki. This study was approved by the ethics committee of The University of Queensland (HREC/09/QRBW/14) and the Ochsner Medical Foundation (USA). Written informed consent was obtained from the participants at the Ochsner Baptist Medical Center (New Orleans, USA).

Samples were obtained before 18 weeks of gestation and classified according to the pregnancy outcomes as normal, PE, GDM, PTB, or other complications (excluding PE, GDM, and PTB). PE was defined as new-onset hypertension (BP ≥ 140/90 mmHg on two separate occasions at least 6 hours apart or BP ≥ 160/110 mmHg) and proteinuria (>300 mg/24 hours) after 20 weeks of gestation in previously normotensive individuals, according to the International Society for the Study of Hypertension in Pregnancy (*54*). A two-step approach was used to screen GDM, including a 50-g oral glucose challenge test performed in a non-fasting state between 24 and 28 weeks of gestation. If the screening threshold was met or exceeded, then patients underwent an OGTT: A fasting glucose level was obtained, a 75- or 100-g glucose load was administered, and glucose levels were evaluated after 1, 2, and 3 hours. GDM was diagnosed when two or more glucose values were greater than or equal to specified thresholds (*55*). PTB was defined as birth before gestational week 37 + 0. After informed consent was obtained, 10 ml of blood was collected by peripheral venipuncture, allowed to clot upright for at least 20 min at room temperature, and centrifuged at 2000*g* for 10 min. The plasma was removed, aliquoted into 0.5 ml of serum, and stored at −80°C. The clinical characteristics of the patients included in this study are shown in Table 1.

Extracellular vesicle isolation

The EVs were isolated using a size exclusion chromatography column coupled with HPLC. Briefly, the Prominence modular HPLC

system from Shimadzu was configured with an autoinjector with space for 70 samples (catalog no. 228-4467-92) and a fraction collector (FRC-10A). The system was connected to a size exclusion chromatography column with a 1-ml volume. The autoinjector and fraction collector were temperature-controlled at 4°C throughout the purification procedure to ensure sample integrity. The samples were subjected to low-speed centrifugation at 2000*g* for 30 min, followed by centrifugation at 12,000*g* for 40 min to remove cell debris and large vesicles. They were then aliquoted into glass vials and placed in a chilled autoinjector for further processing. During the sample injection step, 100 μl of samples were injected into the system. The mobile phase comprised Dulbecco's PBS (DPBS; Thermo Fisher Scientific) at 0.5 ml/min; the absorbance was monitored at 280 nm. Fractions were collected every 1 min (0.5 ml) using a fraction collector and stored at −80°C before evaluation for EVs. Upon completion of each fractionation step, a cleaning-in-place process was performed by switching the mobile phase to 30% isopropanol/1 M NaOH at 0.5 ml/min to remove serum proteins bound to the column, which were then re-equilibrated with DPBS for the next sample injection. The pellet was dissolved in filtered PBS and stored at −80°C. The EVs were then characterized according to the MISEV guidelines, based on their size distribution (NTA), morphology (images were obtained by cryo-TEM), and abundance of the proteins associated with these EVs: CD63, CD81, and CD9 (ExoView R100, NanoView Biosciences).

Target peptide set selection for placental extracellular vesicles

CD9, CD63, CD81, and TSG101, involved in the biogenesis and trafficking of EVs and PLAP, were selected to target circulating placental EVs on the basis of previous studies (*46*, *56*). The FASTA protein sequences for all proteins were imported into Skyline software (version 20.2.1.404) for method development and data processing as previously described (*57*). A targeted Multiple Reaction Monitoring High-Resolution (MR-MHR) experiment was performed using the preselected peptides and their corresponding masses to select the optimal fragment ions. The tryptic peptides were injected into a TripleTOF 5600 mass spectrometer (AbSciex) connected to a NanoLC 400 system using an analytical MicroLC column (ChromXP C18CL, 120A, 150 mm by 0.3 mm (Eksigent). Chromatography was performed in trap-elution mode using solvent A (100% H_2O, 0.1% formic acid) and solvent B (100% acetonitrile, 0.1% formic acid). Peptide separation was performed at a flow rate of 0.25 μl/ml according to the gradient conditions in table S8. Subsequently, full-scan data were extracted from the raw data. Wiff files were created using SkyLine software. The fragment ions were manually inspected, and consecutive high-mass *y*-ion series provided evidence for correct peptide identification. The top three fragment ions were selected for the MRM experiment on the basis of their highest co-elution ion intensities. MRM experiments were performed using a 5500 QTRAP hybrid triple quadrupole/linear ion trap mass spectrometer (AB Sciex) equipped with an Eksigent MicroLC 200 system.

Protein structures

Human CD9, PLAP, CD63, CD81, and TSG101 AlphaFold (*58*) were downloaded from UniProt (*59*) with codes P21926, P05187, P08962, P60033, and Q99816, respectively. The peptide residues were selected in the coordinates file, the solvent-accessible surface (SASA) was calculated using the FreeSASA software (*60*), and the secondary structure was determined using DSSP (database of secondary structure assignments in proteins) (*61*). The figures were prepared using Biopython (*62*) and PyMOL (*63*) scripts.

Model construction

The PyCaret classification module trained 14 different algorithms for the two outcomes. PyCaret (version 3.3.2) (*64*) is an automated machine learning low-code library in Python that automates the machine learning workflow. Python (version 3.11.0) was used for all models. By default, a random selection method was used to split the data into training and test sets of 70 and 30%, respectively.

Algorithm selection and performance measures

Fourteen machine learning algorithms were trained: random forest, support vector machine–radial kernel, extra trees classifier, Gaussian process classifier, decision tree classifier, multilayer perceptron, light gradient boosting machine, *K* neighbors classifier, gradient boosting classifier, AdaBoost classifier, logistic regression, linear discriminant analysis, quadratic discriminant analysis, and naïve Bayes. The algorithms were evaluated first on 10-fold cross-validation and then on the test data. The best model was selected on the basis of accuracy, which was calculated as the total number of correct predictions divided by the total number of predictions. In addition, the optimal sensitivity, specificity, PPV, NPV, AUROC, AUPRC, and Brier scores were calculated for the training and test data. Last, feature importance was calculated for the best model, providing an overall assessment of the most crucial biomarkers in distinguishing the control and case samples.

Cell culture

BeWo cells were used as placental cells to analyze the in vitro effects of mimetic exposure on the hyperglycemic microenvironment, inflammatory conditions, and infection signals. These cells were cultured in growth medium nutrient mixture F-12 Ham (Sigma-Aldrich) supplemented with 15% fetal bovine serum (FBS; Gibco) and 1% antimycotic/antibiotic (100×; Thermo Fisher Scientific, MA, USA). To avoid incorporating external EVs into the assay, the media used for the treatment were supplemented with EV-depleted FBS by centrifugation at maximum speed (30,000 rpm) for 20 hours using a SureSpin 630 Swinging Bucket Rotor (Thermo Fisher Scientific). BeWo cells were plated in 12-well clear tissue culture (TC)–treated multiple well plates (Costar) at a cell density of 75,000 cells per well in 1 ml of medium. The cells were cultured at 37°C and 8% O_2. After 24 to 48 hours, the cells reached ~85% confluence, as determined using IncuCyte (CCD-WI-15); confluence was used to normalize exosome release.

Placental cells were tested before and after syncytialization and treated with forskolin (20 μM). Using a pipette, cells were washed twice with 300 μl of DPBS (Thermo Fisher Scientific) and aspirated. Then, forskolin was added to a final concentration of 20 μM (1.7 μl of standard per milliliter of medium). BeWo cells were treated with different concentrations of lipopolysaccharide from *Escherichia coli* 0111:B4 strain concentrations of 0, 0.01, 0.1, 1, and 10 μg/ml. Tumor necrosis factor–α (R&D Systems) was used in the following concentrations: 0.002, 0.02, 0.2, 2, and 20 ng/ml. Glucose (Gibco) was used for the glucose treatment, considering that the normal growth medium contained 5 mM glucose. In the presence of high glucose concentrations, 20 mM glucose was used. The glucose assay also included an osmotic control. Experiments at normal and high glucose

levels were performed in the presence or absence of insulin 1 nM (Sigma-Aldrich).

Collection of cell-conditioned medium and cell lysate

After 48 hours of treatment, cell confluence was determined using the IncuCyte reagent (Essen Biosciences). The supernatant was collected and centrifuged (sample E). The wells were washed with 1 ml of DPBS and then treated with 100 µl of radioimmunoprecipitation assay buffer (Sigma-Aldrich). Separately, the wells were scratched, and the lysate was collected in a microcentrifuge tube (Neptune). The microcentrifuge tube containing the lysate was sonicated in an ultrasonic unit (Elma Elmasonic S15H) for 5 min (sample C).

Sample E was centrifuged at 2000*g* for 10 min. The supernatant was transferred to a different microcentrifuge tube and centrifuged at 12,000*g* for 10 min. The supernatants were stored for exosome isolation. Sample C was centrifuged at 12,000*g* for 15 min. The supernatants were stored for protein quantification and western blot analysis.

Superparamagnetic SMNF synthesis

Flower-like SMNFs was prepared using the solvothermal method. In a typical process, $Ni(NO_3)_2{\cdot}6H_2O$ (0.5 mM) was dissolved in 40 ml of isopropanol, followed by the addition of $Fe(NO_3)_3{\cdot}9H_2O$ (1 mM). Glycerol (8 ml) was slowly added to the solution under magnetic stirring for 1 hour. The resulting solution was transferred to a 100-ml Teflon-lined stainless-steel autoclave and heated at 180°C for 16 hours in an electric oven. The product was collected by centrifugation (1000 rpm for 10 min), washed thrice with ethanol, and dried in an oven at 60°C for 5 hours. The greenish powder was then subjected to calcination at 350°C for 2 hours in an electric oven.

SMNF-based direct EV isolation

Freshly prepared PLAP-SMNFs (5.0 µl) were mixed with 100 µl of cell culture medium (from BeWo cells) and incubated for 1 hour at room temperature. The SMNF-captured EVs were then washed with 2× binding and washing buffer [10 mM tris-HCl (pH 7.5), 1 mM EDTA, and 2 M NaCl] to remove cell debris and other contaminants. After magnetic washing, the PLAP-SMNF/EV conjugates were transferred to an anti-CD9 antibody-modified glass substrate for naked-eye and colorimetric readouts.

Nanozymatic detection of isolated EVs

The biotinylated anti-CD9 antibody (5.0 µl; 100 ng/ml) was first incubated on the 4-flex glass surface for 30 min. The glass substrate was then washed thrice with PBS to remove loosely attached or unattached CD9 antibodies. To avoid nonspecific binding of EVs or other biomolecules, the glass surface was incubated with a 2% bovine serum albumin solution (as a blocking agent) for 15 min. Next, 5.0 µl of isolated anti-PLAP antibody/SMNF/EV conjugates were added to the glass surface and incubated for 30 min. Last, 50 µl of freshly prepared TMB substrate solution [700 µM TMB and 500 mM H_2O_2 in 0.2 M NaAc buffer (pH 3.5)] was added and incubated for 10 min in the dark to allow the SMNF-catalyzed TMB oxidation reaction to proceed. Color changes were monitored using naked-eye observation. The absorbance was recorded at 650 nm using a SpectraMax spectrophotometer for quantitative measurements. At least three replicates were performed for each standard sample. All measurements were performed at room temperature.

Statistical analysis

Clinical data were analyzed using Student's *t* test, Mann-Whitney *U* test, or Fisher's exact test using SPSS version 25. Hierarchical clustering was performed and displayed using the Qlucore Omics Explorer Software (Qlucore, Lund, Sweden) to visualize the candidate proteins/peptides identified using the probabilistic estimation of expression residuals (PEER) process. Clustering and enrichment of the 110 bivariate biomarkers were performed using cumulative distribution function (CDF). We calculated the statistical power for each protein and sensor comparison using the mean and SD from proteomics and sensor measurements (table S7). The significance level was set at $\alpha = 0.05$, and the statistical power was determined using a *t* test with the "pwrss" R package.

Supplementary Materials

This PDF file includes:

Supplementary Text
Figs. S1 to S12
Tables S1 to S8

REFERENCES AND NOTES

1. H. D. McIntyre, P. Catalano, C. Zhang, G. Desoye, E. R. Mathiesen, P. Damm, Gestational diabetes mellitus. *Nat. Rev. Dis. Primers.* **5**, 47 (2019).
2. E. Dimitriadis, D. L. Rolnik, W. Zhou, G. Estrada-Gutierrez, K. Koga, R. P. V. Francisco, C. Whitehead, J. Hyett, F. da Silva Costa, K. Nicolaides, E. Menkhorst, Pre-eclampsia. *Nat. Rev. Dis. Primers.* **9**, 8 (2023).
3. R. J. Kaaja, I. A. Greer, Manifestations of chronic disease during pregnancy. *JAMA* **294**, 2751–2757 (2005).
4. R. Haddad-Tóvolli, M. Claret, Metabolic and feeding adjustments during pregnancy. *Nat. Rev. Endocrinol.* **19**, 564–580 (2023).
5. M. Attwaters, Detecting pregnancy complications from blood. *Nat. Rev. Genet.* **23**, 136–136 (2022).
6. K. K. Venkatesh, A. M. Perak, J. Wu, P. Catalano, J. L. Josefon, M. M. Costantine, M. B. Landon, N. Lancki, D. Scholtens, W. Lowe, S. S. Khan, W. A. Grobman, Impact of hypertensive disorders of pregnancy and gestational diabetes mellitus on offspring cardiovascular health in early adolescence. *Am. J. Obstet. Gynecol.* **232**, 218.e1–218.e12 (2024).
7. W. L. Lowe Jr., D. M. Scholtens, A. Kuang, B. Linder, J. M. Lawrence, Y. Lebenthal, D. McCance, J. Hamilton, M. Nodzenski, O. Talbot, W. J. Brickman, P. Clayton, R. C. Ma, W. H. Tam, A. R. Dyer, P. M. Catalano, L. P. Lowe, B. E. Metzger, HAPO Follow-up Study Cooperative Research Group, Hyperglycemia and Adverse Pregnancy Outcome Follow-up Study (HAPO FUS): Maternal gestational diabetes mellitus and childhood glucose metabolism. *Diabetes Care* **42**, 372–380 (2019).
8. M. L. Mongraw-Chaffin, P. M. Cirillo, B. A. Cohn, Preeclampsia and cardiovascular disease death: Prospective evidence from the child health and development studies cohort. *Hypertension* **56**, 166–171 (2010).
9. M. V. Diaz-Santana, K. M. O'Brien, Y.-M. M. Park, D. P. Sandler, C. R. Weinberg, Persistence of risk for type 2 diabetes after gestational diabetes mellitus. *Diabetes Care* **45**, 864–870 (2022).
10. Y. Couch, E. I. Buzàs, D. Di Vizio, Y. S. Gho, P. Harrison, A. F. Hill, J. Lötvall, G. Raposo, P. D. Stahl, C. Théry, K. W. Witwer, D. R. F. Carter, A brief history of nearly EV-erything – The rise and rise of extracellular vesicles. *J. Extracell. Vesicles* **10**, e12144 (2021).
11. S. Das, C. J. Lyon, T. Hu, A panorama of extracellular vesicle applications: From biomarker detection to therapeutics. *ACS Nano* **18**, 9784–9797 (2024).
12. C. Salomon, S. Das, U. Erdbrügger, R. Kalluri, S. K. Lim, J. M. Olefsky, G. E. Rice, S. Sahoo, W. A. Tao, P. Vader, Q. Wang, A. M. Weaver, Extracellular vesicles and their emerging roles as cellular messengers in endocrinology: An endocrine society scientific statement. *Endocr. Rev.* **43**, 441–468 (2022).
13. C. Salomon, K. Scholz-Romero, S. Sarker, E. Sweeney, M. Kobayashi, P. Correa, S. Longo, G. Duncombe, M. D. Mitchell, G. E. Rice, S. E. Illanes, Gestational diabetes mellitus is associated with changes in the concentration and bioactivity of placenta-derived exosomes in maternal circulation across gestation. *Diabetes* **65**, 598–609 (2016).
14. R. A. Dragovic, G. P. Collett, P. Hole, D. J. P. Ferguson, C. W. Redman, I. L. Sargent, D. S. Tannetta, Isolation of syncytiotrophoblast microvesicles and exosomes and their characterisation by multicolour flow cytometry and fluorescence Nanoparticle Tracking Analysis. *Methods* **87**, 64–74 (2015).

15. C. Motta-Mejia, N. Kandzija, W. Zhang, V. Mhlomi, A. S. Cerdeira, A. Burdujan, D. Tannetta, R. Dragovic, I. L. Sargent, C. W. Redman, U. Kishore, M. Vatish, Placental vesicles carry active endothelial nitric oxide synthase and their activity is reduced in preeclampsia. *Hypertension* **70**, 372–381 (2017).
16. E. Delorme-Axford, R. B. Donker, J.-F. Mouillet, T. Chu, A. Bayer, Y. Ouyang, T. Wang, D. B. Stolz, S. N. Sarkar, A. E. Morelli, Y. Sadovsky, C. B. Coyne, Human placental trophoblasts confer viral resistance to recipient cells. *Proc. Natl. Acad. Sci. U.S.A.* **110**, 12048–12053 (2013).
17. J. A. Welsh, D. C. I. Goberdhan, L. O'Driscoll, E. I. Buzas, C. Blenkiron, B. Bussolati, H. Cai, D. D. Vizio, T. A. P. Driedonks, U. Erdbrügger, J. M. Falcon-Perez, Q.-L. Fu, A. F. Hill, M. Lenassi, S. K. Lim, M. G. Mahoney, S. Mohanty, A. Möller, R. Nieuwland, T. Ochiya, S. Sahoo, A. C. Torrecilhas, L. Zheng, A. Zijlstra, S. Abuelreich, R. Bagabas, P. Bergese, E. M. Bridges, M. Brucale, D. Burger, R. P. Carney, E. Cocucci, R. Crescitelli, E. Hanser, A. L. Harris, N. J. Haughey, A. Hendrix, A. R. Ivanov, T. Jovanovic-Talisman, N. A. Kruh-Garcia, V. Ku'ulei-Lyn Faustino, D. Kyburz, C. Lässer, K. M. Lennon, J. Lötvall, A. L. Maddox, E. S. Martens-Uzunova, R. R. Mizenko, L. A. Newman, A. Ridolfi, E. Rohde, T. Rojalin, A. Rowland, A. Saftics, U. S. Sandau, J. A. Saugstad, F. Shekari, S. Swift, D. Ter-Ovanesyan, J. P. Tosar, Z. Useckaite, F. Valle, Z. Varga, E. van der Pol, M. J. C. van Herwijnen, M. H. M. Wauben, A. M. Wehman, S. Williams, A. Zendrini, A. J. Zimmerman, MISEV Consortium, C. Théry, K. W. Witwer, Minimal information for studies of extracellular vesicles (MISEV2023): From basic to advanced approaches. *J. Extracell. Vesicles* **13**, e12404 (2024).
18. S. Sharma, M. K. Masud, Y. V. Kaneti, P. Rewatkar, A. Koradia, M. S. A. Hossain, Y. Yamauchi, A. Popat, C. Salomon, Extracellular vesicle nanoarchitectonics for novel drug delivery applications. *Small* **17**, 2102220 (2021).
19. Y. Kang, M. K. Masud, Y. Guo, Y. Zhao, Z. S. Nishat, J. Zhao, B. Jiang, Y. Sugahara, T. Pejovic, T. Morgan, M. S. A. Hossain, H. Li, C. Salomon, T. Asahi, Y. Yamauchi, Au-loaded superparamagnetic mesoporous bimetallic CoFeB nanovehicles for sensitive autoantibody detection. *ACS Nano* **17**, 3346–3357 (2023).
20. M. K. Masud, J. Na, M. Younus, M. S. A. Hossain, Y. Bando, M. J. A. Shiddiky, Y. Yamauchi, Superparamagnetic nanoarchitectures for disease-specific biomarker detection. *Chem. Soc. Rev.* **48**, 5717–5751 (2019).
21. K. Boriachek, M. K. Masud, C. Palma, H. P. Phan, Y. Yamauchi, M. S. A. Hossain, N. T. Nguyen, C. Salomon, M. J. A. Shiddiky, Avoiding pre-isolation step in exosome analysis: Direct isolation and sensitive detection of exosomes using gold-loaded nanoporous ferric oxide nanozymes. *Anal. Chem.* **91**, 3827–3834 (2019).
22. J. Jin, R. Menon, Placental exosomes: A proxy to understand pregnancy complications. *Am. J. Reproduc. Immunol.* **79**, e12788 (2018).
23. C. Théry, K. W. Witwer, E. Aikawa, M. J. Alcaraz, J. D. Anderson, R. Andriantsitohaina, A. Antoniou, T. Arab, F. Archer, G. K. Atkin-Smith, D. C. Ayre, J.-M. Bach, D. Bachurski, H. Baharvand, L. Balaj, S. Baldacchino, N. N. Bauer, A. A. Baxter, M. Bebawy, C. Beckham, A. B. Zavec, A. Benmoussa, A. C. Berardi, P. Bergese, E. Bielska, C. Blenkiron, S. Bobis-Wozowicz, E. Boilard, W. Boireau, A. Bongiovanni, F. E. Borràs, S. Bosch, C. M. Boulanger, X. Breakefield, A. M. Breglio, M. Á. Brennan, D. R. Brigstock, A. Brisson, M. L. D. Broekman, J. F. Bromberg, P. Bryl-Górecka, S. Buch, A. H. Buck, D. Burger, S. Busatto, D. Buschmann, B. Bussolati, E. I. Buzás, J. B. Byrd, G. Camussi, D. R. F. Carter, S. Caruso, L. W. Chamley, Y.-T. Chang, C. Chen, S. Chen, L. Cheng, A. R. Chin, A. Clayton, S. P. Clerici, A. Cocks, E. Cocucci, R. J. Coffey, A. Cordeiro-da-Silva, Y. Couch, F. A. W. Coumans, B. Coyle, R. Crescitelli, M. F. Criado, C. D'Souza-Schorey, S. Das, A. D. Chaudhuri, P. de Candia, E. F. De Santana Junior, O. De Wever, H. A. del Portillo, T. Demaret, S. Deville, A. Devitt, B. Dhondt, D. D. Vizio, L. C. Dieterich, V. Dolo, A. P. D. Rubio, M. Dominici, M. R. Dourado, T. A. P. Driedonks, F. V. Duarte, H. M. Duncan, R. M. Eichenberger, K. Ekström, S. E. L. Andaloussi, C. Elie-Caille, U. Erdbrügger, J. M. Falcón-Pérez, F. Fatima, J. E. Fish, M. Flores-Bellver, A. Försönits, A. Frelet-Barrand, F. Fricke, G. Fuhrmann, S. Gabrielsson, A. Gámez-Valero, C. Gardiner, K. Gärtner, R. Gaudin, Y. S. Gho, B. Giebel, C. Gilbert, M. Gimona, I. Giusti, D. C. I. Goberdhan, A. Görgens, S. M. Gorski, D. W. Greening, J. C. Gross, A. Gualerzi, G. N. Gupta, D. Gustafson, A. Handberg, R. A. Haraszti, P. Harrison, H. Hegyesi, A. Hendrix, A. F. Hill, F. H. Hochberg, K. F. Hoffmann, B. Holder, H. Holthofer, B. Hosseinkhani, G. Hu, Y. Huang, V. Huber, S. Hunt, A. G.-E. Ibrahim, T. Ikezu, J. M. Inal, M. Isin, A. Ivanova, H. K. Jackson, S. Jacobsen, S. M. Jay, M. Jayachandran, G. Jenster, L. Jiang, S. M. Johnson, J. C. Jones, A. Jong, T. Jovanovic-Talisman, S. Jung, R. Kalluri, S.-I. Kano, S. Kaur, Y. Kawamura, E. T. Keller, D. Khamari, E. Khomyakova, A. Khvorova, P. Kierulf, K. P. Kim, T. Kislinger, M. Klingeborn, D. J. Klinke II, M. Kornek, M. M. Kosanović, Á. F. Kovács, E.-M. Krämer-Albers, S. Krasemann, M. Krause, I. V. Kurochkin, G. D. Kusuma, S. Kuypers, S. Laitinen, S. M. Langevin, L. R. Languino, J. Lannigan, C. Lässer, L. C. Laurent, G. Lavieu, E. Lázaro-Ibáñez, S. L. Lay, M.-S. Lee, Y. X. F. Lee, D. S. Lemos, M. Lenassi, A. Leszczynska, I. T. Li, K. Liao, S. F. Libregts, E. Ligeti, R. Lim, S. K. Lim, A. Linē, K. Linnemannstöns, A. Llorente, C. A. Lombard, M. J. Lorenowicz, Á. M. Lörincz, J. Lötvall, J. Lovett, M. C. Lowry, X. Loyer, Q. Lu, B. Lukomska, T. R. Lunavat, S. L. N. Maas, H. Malhi, A. Marcilla, J. Mariani, J. Mariscal, E. S. Martens-Uzunova, L. Martin-Jaular, M. C. Martinez, V. R. Martins, M. Mathieu, S. Mathivanan, M. Maugeri, L. K. McGinnis, M. J. McVey, D. G. Meckes Jr., K. L. Meehan, I. Mertens, V. R. Minciacchi, A. Möller, M. M. Jørgensen, A. Morales-Kastresana, J. Morhayim, F. Mullier, M. Muraca, L. Musante, V. Mussack, D. C. Muth, K. H. Myburgh, T. Najrana, M. Nawaz, I. Nazarenko, P. Nejsum, C. Neri, T. Neri, R. Nieuwland, L. Nimrichter, J. P. Nolan, E. N. M. N. Hoen, N. N. Hooten, L. O'Driscoll, T. O'Grady, A. O'Loghlen, T. Ochiya, M. Olivier, A. Ortiz, L. A. Ortiz, X. Osteikoetxea, O. Østergaard, M. Ostrowski, J. Park, D. M. Pegtel, H. Peinado, F. Perut, M. W. Pfaffl, D. G. Phinney, B. C. H. Pieters, R. C. Pink, D. S. Pisetsky, E. P. von Strandmann, I. Polakovicova, I. K. H. Poon, B. H. Powell, I. Prada, L. Pulliam, P. Quesenberry, A. Radeghieri, R. L. Raffai, S. Raimondo, J. Rak, M. I. Ramirez, G. Raposo, M. S. Rayyan, N. Regev-Rudzki, F. L. Ricklefs, P. D. Robbins, D. D. Roberts, S. C. Rodrigues, E. Rohde, S. Rome, K. M. A. Rouschop, A. Rughetti, A. E. Russell, P. Saá, S. Sahoo, E. Salas-Huenuleo, C. Sánchez, J. A. Saugstad, M. J. Saul, R. M. Schiffelers, R. Schneider, T. H. Schøyen, A. Scott, E. Shahaj, S. Sharma, O. Shatnyeva, F. Shekari, G. V. Shelke, A. K. Shetty, K. Shiba, P. R.-M. Siljander, A. M. Silva, A. Skowronek, O. L. Snyder II, R. P. Soares, B. W. Sódar, C. Soekmadji, J. Sotillo, P. D. Stahl, W. Stoorvogel, S. L. Stott, E. F. Strasser, S. Swift, H. Tahara, M. Tewari, K. Timms, S. Tiwari, R. Tixeira, M. Tkach, W. S. Toh, R. Tomasini, A. C. Torrecilhas, J. P. Tosar, V. Toxavidis, L. Urbanelli, P. Vader, B. W. M. van Balkom, S. G. van der Grein, J. Van Deun, M. J. C. van Herwijnen, K. Van Keuren-Jensen, G. van Niel, M. E. van Royen, A. J. van Wijnen, M. H. Vasconcelos, I. J. Vechetti Jr., T. D. Veit, L. J. Vella, É. Velot, F. J. Verweij, B. Vestad, J. L. Viñas, T. Visnovitz, K. V. Vukman, J. Wahlgren, D. C. Watson, M. H. M. Wauben, A. Weaver, J. P. Webber, V. Weber, A. M. Wehman, D. J. Weiss, J. A. Welsh, S. Wendt, A. M. Wheelock, Z. Wiener, L. Witte, J. Wolfram, A. Xagorari, P. Xander, J. Xu, X. Yan, M. Yáñez-Mó, H. Yin, Y. Yuana, V. Zappulli, J. Zarubova, V. Žėkas, J.-Y. Zhang, Z. Zhao, L. Zheng, A. R. Zheutlin, A. M. Zickler, P. Zimmermann, A. M. Zivkovic, D. Zocco, E. K. Zuba-Surma, Minimal information for studies of extracellular vesicles 2018 (MISEV2018): A position statement of the International Society for Extracellular Vesicles and update of the MISEV2014 guidelines. *J. Extracell. Vesicles* **7**, 1535750 (2018).
24. Y. Tian, M. Gong, Y. Hu, H. Liu, W. Zhang, M. Zhang, X. Hu, D. Aubert, S. Zhu, L. Wu, X. Yan, Quality and efficiency assessment of six extracellular vesicle isolation methods by nano-flow cytometry. *J. Extracell. Vesicles* **9**, 1697028 (2020).
25. C. Liu, H. Lin, H. Yu, X. Mai, W. Pan, J. Guo, T. Liao, J. Feng, Y. Zhang, B. Situ, L. Zheng, B. Li, Isolation and enrichment of extracellular vesicles with double-positive membrane protein for subsequent biological studies. *Adv. Healthc. Mater.* **13**, e2303430 (2024).
26. N.-E. Onukwugha, Y.-T. Kang, S. Nagrath, Emerging micro-nanotechnologies for extracellular vesicles in immuno-oncology: From target specific isolations to immunomodulation. *Lab Chip* **22**, 3314–3339 (2022).
27. W. Yang, Y. Yu, X. Shou, D. Zhang, G. Liang, Y. Zhao, Hedgehog-inspired magnetic nanoparticles for effectively capturing and detecting exosomes. *NPG Asia Mater.* **13**, 78 (2021).
28. M. K. Masud, J. Kim, M. M. Billah, K. Wood, M. J. A. Shiddiky, N.-T. Nguyen, R. K. Parsapur, Y. V. Kaneti, A. A. Alshehri, Y. G. Alghamidi, K. A. Alzahrani, M. Adharvanachari, P. Selvam, M. S. Hossain, Y. Yamauchi, Nanoarchitectured peroxidase-mimetic nanozymes: Mesoporous nanocrystalline α-or γ-iron oxide? *J. Mater. Chem. B* **7**, 5412–5422 (2019).
29. P. Guardia, A. Labarta, X. Batlle, Tuning the size, the shape, and the magnetic properties of iron oxide nanoparticles. *J. Phys. Chem. C* **115**, 390–396 (2011).
30. F. J. Owens, Ferromagnetic resonance observation of a phase transition in magnetic field-aligned Fe_2O_3 nanoparticles. *J. Magnet. Magnetic Mater.* **321**, 2386–2391 (2009).
31. M. Broto, M. M. Kaminski, C. Adrianus, N. Kim, R. Greensmith, S. Dissanayake-Perera, A. J. Schubert, X. Tan, H. Kim, A. S. Dighe, J. J. Collins, M. M. Stevens, Nanozyme-catalysed CRISPR assay for preamplification-free detection of non-coding RNAs. *Nat. Nanotechnol.* **17**, 1120–1126 (2022).
32. Y. Ouyang, M. P. O'Hagan, I. Willner, Functional catalytic nanoparticles (nanozymes) for sensing. *Biosens. Bioelectron.* **218**, 114768 (2022).
33. M. Huo, L. Wang, H. Zhang, L. Zhang, Y. Chen, J. Shi, Construction of single-iron-atom nanocatalysts for highly efficient catalytic antibiotics. *Small* **15**, 1901834 (2019).
34. Y. Ouyang, M. Fadeev, P. Zhang, R. Carmieli, J. Li, Y. S. Sohn, O. Karmi, R. Nechushtai, E. Pikarsky, C. Fan, I. Willner, Aptamer-modified Au nanoparticles: Functional nanozyme bioreactors for cascaded catalysis and catalysts for chemodynamic treatment of cancer cells. *ACS Nano* **16**, 18232–18243 (2022).
35. S. Sarker, K. Scholz-Romero, A. Perez, S. E. Illanes, M. D. Mitchell, G. E. Rice, C. Salomon, Placenta-derived exosomes continuously increase in maternal circulation over the first trimester of pregnancy. *J. Transl. Med.* **12**, 204 (2014).
36. O. Elfeky, S. Longo, A. Lai, G. E. Rice, C. Salomon, Influence of maternal BMI on the exosomal profile during gestation and their role on maternal systemic inflammation. *Placenta* **50**, 60–69 (2017).
37. S. N. Hinkle, M. Y. Tsai, S. Rawal, P. S. Albert, C. Zhang, HbA1c measured in the first trimester of pregnancy and the association with gestational diabetes. *Sci. Rep.* **8**, 12249 (2018).
38. S. Riskin-Mashiah, G. Younes, A. Damti, R. Auslender, First-trimester fasting hyperglycemia and adverse pregnancy outcomes. *Diabetes Care* **32**, 1639–1643 (2009).
39. C. L. Meek, H. R. Murphy, D. Simmons, Random plasma glucose in early pregnancy is a better predictor of gestational diabetes diagnosis than maternal obesity. *Diabetologia* **59**, 445–452 (2016).

40. A. N. Sweeting, H. Appelblom, G. P. Ross, J. Wong, H. Kouru, P. F. Williams, M. Sairanen, J. A. Hyett, First trimester prediction of gestational diabetes mellitus: A clinical model based on maternal demographic parameters. *Diabetes Res. Clin. Pract.* **127**, 44–50 (2017).
41. S. Bhattacharya, L. Nagendra, D. Dutta, S. Mondal, S. Bhat, J. M. Raj, H. Boro, A. B. M. Kamrul-Hasan, S. Kalra, First-trimester fasting plasma glucose as a predictor of subsequent gestational diabetes mellitus and adverse fetomaternal outcomes: A systematic review and meta-analysis. *Diabetes Metab. Syndr.* **18**, 103051 (2024).
42. J.-N. Tong, L.-L. Wu, Y.-X. Chen, X.-N. Guan, F.-Y. Tian, H.-F. Zhang, K. Liu, A.-Q. Yin, X.-X. Wu, J.-M. N. Prof, Fasting plasma glucose in the first trimester is related to gestational diabetes mellitus and adverse pregnancy outcomes. *Endocrine* **75**, 70–81 (2022).
43. C. Salomon, M. J. Torres, M. Kobayashi, K. Scholz-Romero, L. Sobrevia, A. Dobierzewska, S. E. Illanes, M. D. Mitchell, G. E. Rice, A gestational profile of placental exosomes in maternal plasma and their effects on endothelial cell migration. *PLOS ONE* **9**, e98667 (2014).
44. S. Adam, O. Elfeky, V. Kinhal, S. Dutta, A. Lai, N. Jayabalan, Z. Nuzhat, C. Palma, G. E. Rice, C. Salomon, Review: Fetal-maternal communication via extracellular vesicles - Implications for complications of pregnancies. *Placenta* **54**, 83–88 (2017).
45. S. Nair, M. Razo-Azamar, N. Jayabalan, L. T. Dalgaard, B. Palacios-González, A. Sørensen, U. Kampmann, A. Handberg, F. Carrion, C. Salomon, Advances in extracellular vesicles as mediators of cell-to-cell communication in pregnancy. *Cytokine Growth Factor Rev.* **76**, 86–98 (2024).
46. C. Salomon, D. Guanzon, K. Scholz-Romero, S. Longo, P. Correa, S. E. Illanes, G. E. Rice, Placental exosomes as early biomarker of preeclampsia: Potential role of exosomal microRNAs across gestation. *J. Clin. Endocrinol. Metab.* **102**, 3182–3194 (2017).
47. R. Menon, C. Debnath, A. Lai, D. Guanzon, S. Bhatnagar, P. K. Kshetrapal, S. Sheller-Miller, C. Salomon, Garbhini Study Team, Circulating exosomal miRNA profile during term and preterm birth pregnancies: A longitudinal study. *Endocrinology* **160**, 249–275 (2019).
48. J. Miranda, C. Paules, S. Nair, A. Lai, C. Palma, K. Scholz-Romero, G. E. Rice, E. Gratacos, F. Crispi, C. Salomon, Placental exosomes profile in maternal and fetal circulation in intrauterine growth restriction - Liquid biopsies to monitoring fetal growth. *Placenta* **64**, 34–43 (2018).
49. N. Jayabalan, A. Lai, S. Nair, D. Guanzon, K. Scholz-Romero, C. Palma, H. D. McIntyre, M. Lappas, C. Salomon, Quantitative proteomics by SWATH-MS suggest an association between circulating exosomes and maternal metabolic changes in gestational diabetes mellitus. *Proteomics* **19**, 1800164 (2019).
50. G. Truong, D. Guanzon, V. Kinhal, O. Elfeky, A. Lai, S. Longo, Z. Nuzhat, C. Palma, K. Scholz-Romero, R. Menon, B. W. Mol, G. E. Rice, C. Salomon, Oxygen tension regulates the miRNA profile and bioactivity of exosomes released from extravillous trophoblast cells - Liquid biopsies for monitoring complications of pregnancy. *PLOS ONE* **12**, e0174514 (2017).
51. L. B. James-Allan, F. J. Rosario, K. Barner, A. Lai, D. Guanzon, H. D. McIntyre, M. Lappas, T. L. Powell, C. Salomon, T. Jansson, Regulation of glucose homeostasis by small extracellular vesicles in normal pregnancy and in gestational diabetes. *FASEB J.* **34**, 5724–5739 (2020).
52. A. Yokoi, M. Ukai, T. Yasui, Y. Inokuma, K. Hyeon-Deuk, J. Matsuzaki, K. Yoshida, M. Kitagawa, K. Chattrairat, M. Iida, T. Shimada, Y. Manabe, I.-Y. Chang, E. Asano-Inami, Y. Koya, A. Nawa, K. Nakamura, T. Kiyono, T. Kato, A. Hirakawa, Y. Yoshioka, T. Ochiya, T. Hasegawa, Y. Baba, Y. Yamamoto, H. Kajiyama, Identifying high-grade serous ovarian carcinoma–specific extracellular vesicles by polyketone-coated nanowires. *Sci. Adv.* **9**, eade6958 (2023).
53. W. Yang, Y. Yu, X. Shou, D. Zhang, G. Liang, Y. Zhao, Hedgehog-inspired magnetic nanoparticles for effectively capturing and detecting exosomes. *NPG Asia Mater* **13**, 78 (2021).
54. L. A. Magee, M. A. Brown, D. R. Hall, S. Gupte, A. Hennessy, S. A. Karumanchi, L. C. Kenny, F. McCarthy, J. Myers, L. C. Poon, S. Rana, S. Saito, A. C. Staff, E. Tsigas, P. von Dadelszen, The 2021 International Society for the Study of Hypertension in Pregnancy classification, diagnosis & management recommendations for international practice. *Pregnancy Hypertens.* **27**, 148–169 (2022).
55. Committee on Practice Bulletins—Obstetrics, Practice bulletin no. 137: Gestational diabetes mellitus. *Obstet. Gynecol.* **122**, 406–416 (2013).
56. M. D. Mitchell, H. N. Peiris, M. Kobayashi, Y. Q. Koh, G. Duncombe, S. E. Illanes, G. E. Rice, C. Salomon, Placental exosomes in normal and complicated pregnancy. *Am. J. Obstet. Gynecol.* **213**, S173–S181 (2015).
57. M. Alharbi, A. Lai, S. Sharma, P. Kalita-de Croft, N. Godbole, A. Campos, D. Guanzon, A. Salas-Burgos, F. Carrion, F. A. Zuñiga, L. Perrin, Y. He, T. Pejovic, C. Winters, T. Morgan, J. D. Hooper, G. E. Rice, C. Salomon, Extracellular vesicle transmission of chemoresistance to ovarian cancer cells is associated with hypoxia-induced expression of glycolytic pathway proteins, and prediction of epithelial ovarian cancer disease recurrence. *Cancer* **13**, 3388 (2021).
58. J. Jumper, R. Evans, A. Pritzel, T. Green, M. Figurnov, O. Ronneberger, K. Tunyasuvunakool, R. Bates, A. Žídek, A. Potapenko, A. Bridgland, C. Meyer, S. A. A. Kohl, A. J. Ballard, A. Cowie, B. Romera-Paredes, S. Nikolov, R. Jain, J. Adler, T. Back, S. Petersen, D. Reiman, E. Clancy, M. Zielinski, M. Steinegger, M. Pacholska, T. Berghammer, S. Bodenstein, D. Silver, O. Vinyals, A. W. Senior, K. Kavukcuoglu, P. Kohli, D. Hassabis, Highly accurate protein structure prediction with AlphaFold. *Nature* **596**, 583–589 (2021).
59. The Unipot Consortium, UniProt: The universal protein knowledgebase in 2023. *Nucleic Acids Res.* **51**, D523–D531 (2023).
60. S. Mitternacht, FreeSASA: An open source C library for solvent accessible surface area calculations. *F1000Research* **5**, 189 (2016).
61. J. Zacharias, E.-W. Knapp, Protein secondary structure classification revisited: Processing DSSP information with PSSC. *J. Chem. Info. Model.* **54**, 2166–2179 (2014).
62. P. J. A. Cock, T. Antao, J. T. Chang, B. A. Chapman, C. J. Cox, A. Dalke, I. Friedberg, T. Hamelryck, F. Kauff, B. Wilczynski, M. J. L. de Hoon, Biopython: Freely available Python tools for computational molecular biology and bioinformatics. *Bioinformatics* **25**, 1422–1423 (2009).
63. Schrodinger LLC, The PyMOL molecular graphics system, version 1.8 (2015).
64. M. Ali, PyCaret: An open source, low-code machine learning library in Python, PyCaret version 2 (2020).

Acknowledgments: This work used the Queensland node of the NCRIS-enabled Australian National Fabrication Facility (ANFF). We thank M. Shahbazi for conducting magnetic measurement of SMNFs. **Funding:** This project was conducted with the support of The National Health and Medical Research Council (NHMRC, 1195451) and the Danish Diabetes and Endocrinology Academy. C.P. received a Ph.D. scholarship from CONICYT PFCHA/ Doctorado Becas Chile/2018 – 72190513. This research was facilitated by access to the Mass Spectrometry Facility at UQ Centre for Clinical Research. M.K.M. supported by the Cancer Council Queensland through a Next Generation Cancer Council fellowship (2027070). We also acknowledge the support from the JST-ERATO Yamauchi Materials Space-Tectonics Project (JPMJER2003); ARC Australian Laureate Fellowship (FL230100095) to Y.Y.; and an ARC Linkage Infrastructure, Equipment, and Facilities (LE230100045) to M.S.A.H. **Author contributions:** C.P.: Writing—original draft, conceptualization, investigation, writing—review and editing, methodology, data curation, validation, formal analysis, project administration, and visualization. M.K.M.: Writing—original draft, conceptualization, investigation, writing—review and editing, methodology, funding acquisition, data curation, and formal analysis. D.G.: Writing—review and editing, data curation, formal analysis, software, and visualization. A.L.: Investigation, writing—review and editing, data curation, and project administration. M.R.: Conceptualization, investigation, writing—review and editing, methodology, and validation. A.N.: Conceptualization, investigation, writing—review and editing, methodology, and validation. S.N.: Writing—review and editing. A.S.-B.: Writing—original draft, writing—review and editing, methodology, data curation, formal analysis, software, and visualization. M.S.A.H.: Investigation, writing—review and editing, resources, funding acquisition, and formal analysis. F.C.: Writing—original draft, conceptualization, and writing—review and editing. G.D.: Conceptualization, investigation, writing—review and editing, resources, and visualization. H.D.M.: Conceptualization, writing—review and editing, and supervision. A.H.: Investigation and writing—review and editing. S.L.: Conceptualization, writing—review and editing, supervision. Y.Y.: Conceptualization, investigation, writing—review and editing, methodology, resources, funding acquisition, validation, supervision, project administration, and visualization. C.S.: Writing—original draft, conceptualization, investigation, writing—review and editing, methodology, resources, funding acquisition, data curation, validation, supervision, formal analysis, software, project administration, and visualization. **Competing interests:** The authors declare that they have no competing interests. **Data and materials availability:** All data needed to evaluate the conclusions in the paper are present in the paper and/or the Supplementary Materials.

Submitted 15 July 2024
Accepted 24 January 2025
Published 26 February 2025
10.1126/sciadv.adr4074